A semi-smooth Newton and Primal–Dual Active Set method for Non-Smooth Contact Dynamics

Stéphane Abide, Mikaël Barboteu, Soufiane Cherkaoui, Serge Dumont

A Semi-Smooth Newton and Primal-Dual Active Set Method for Non-Smooth Contact Dynamics

Stéphane Abide[*], *Mikaël Barboteu*[*1], *Soufiane Cherkaoui*[*] *and Serge Dumont*[#]

stephane.abide@univ-perp.fr, barboteu@univ-perp.fr, soufiane.cherkaoui@univ-perp.fr, serge.dumont@unimes.fr

[*] *Laboratoire de Mathématiques et Physique*
Université de Perpignan Via Domitia
52 Avenue Paul Alduy, 66860 Perpignan, France

[#] *Institut Montpelliérain Alexander Grothendieck*
Université de Nîmes
Site des Carmes, Place Gabriel Péri, 30000 Nîmes, France

Abstract

Multi-rigid-body dynamic contact systems, in other words Non Smooth Contact Dynamics (NSCD) problems, generate some inherent difficulties to multivocal laws, which results in non-linearities and non-smoothness associated to frictional contact models. Recently, Primal-Dual Active Set strategies (PDAS) have emerged as a promising method for solving contact problems. These methods are based on the following principle: the frictional contact conditions are restated as non-linear complementary functions for which the solution is provided by the iterative semi-smooth Newton method. Based on these prerequisites, this contribution aims to provide a generalization of the NSCD-PDAS for dynamic frictional contact problems. Several numerical experiments are reported for algorithm validation purposes and also to assess the efficiency and performances of PDAS methods with respect to the Newton/Augmented Lagrangian and the Bi-Potential methods.

AMS Subject Classification: 70F40, 70-08, 70E55, 35Q70

Keywords: Granular media, Unilateral constraint, Friction, Rigid body, Discrete Element Method, Non-Smooth Contact Dynamics, Semi-Smooth Newton method, Primal-Dual Active Set, Bi-potential method, Augmented Lagrangian method, Multi-rigid-body contact, Numerical simulations.

[1]Corresponding author.

1. Introduction

Predicting snow avalanches, railway ballast track deformations or designing effective process for C02 capture requires taking into account local interactions modeling to assess macroscopic properties. This research issue is particularly topical because of its wide range of applications and the computational resources constantly increasing. As a matter of fact, multi-rigid-body dynamic contact field, as granular materials, illustrates some inherent difficulties to multivocal laws, which results in non-linearities and non-smoothness associated to frictional contact models. Numerical simulations of discrete materials, and specifically granular ones, was first initiated within the framework of the Discrete Element Method (DEM) [1–3]. DEM relies on appropriate regularisation techniques for non-linear contact laws while using an explicit time scheme to ease their numerical treatments. Currently, this approach is still widely used in the engineering process design (see for example the MFIX open source software [4]). Some DEM weaknesses, reported in [2], include the small time steps inherent in the explicit time scheme or the damping introduced for stability matters.

Moreau established the theoretical concepts to properly handle the non-smooth mechanics featured by non-differentiable laws in its common definition. Thus, he introduced the second-order sweeping process as the framework of mathematical analysis and numerical schemes designed for granular materials. The cornerstone is the formulation for the Signorini problem in terms of velocities and impulses, leading to the *Moreau-Jean time-stepping approach* [5]. This numerical scheme is implicit and the energy conservation property holds unlike the DEM framework. The local conditions of contact between rigid bodies are ensured by means of a Non-Linear Gauss-Seidel (NLGS) developed by M. Jean and J. J. Moreau [5–8]. Also, The numerical aspects and certain algorithmic developments for the Non-Smooth Contact Dynamics (NSCD) have been proposes in [9]. Some alternatives such as conjugate gradient solvers have been proposed [10], with a specific analysis for parallel computing [11, 12]. As pointed out by Dubois et al. [2], this non-linear formulation is computationally expensive compared to DEM, especially for compressed granular materials, but larger time steps can be considered. Another point to consider in NSCD is the way to ensure the local contact condition. Usual approaches are based on the bi-potential or the augmented Lagrangian theory [13–15]. Efficiency of such methods strongly depends on the penalty coefficients [14, 16, 17]. Some improvements have been proposed to overcome this issue [18, 19], but they are more time consuming.

Numerical simulations carried out for hyper-elastic bodies with frictional contact have led to specific approaches [16, 20–29]. Recently, Primal-Dual Active Set strategies (PDAS) have emerged as a promising method for solving contact problems (see [30–33]). These methods are based on the following principle: the frictional contact conditions are restated as non-linear complementary functions for which the solution is provided by the iterative semi-smooth Newton method [30, 31]. In practice, contact with Coulomb friction conditions can be formulated in terms of a fixed point problem related to a quasi-optimisation problem.

Therefore, the whole elastic body's problem, including the frictional contacts, consists of successive solutions of many elastic problems with simpler boundary conditions: Dirichlet, Neumann or Robin boundary conditions depending on the pseudo-transient status of the contact nodes [34, 35]. This method is also known as the stabilized or Nitsche's methods [23, 36, 37].

According to our knowledge, few references on Active Set methods for solving muti-rigid-body dynamic contact problems are available. Based on a pseudo-rigid body assumption, Koziara and Bicanic [38] modified a semi-smooth Newton technique to effectively deal with the frictional contact problem. Within a framework of optimization, Sharaf [39] proposes an Active Set method for solving positive definite and positive semi-definite Linear Complementary Problems (LCP). The effectiveness of its approach has been tested on the *toy problem* of static vertical rigid spheres assuming frictionless contacts. The resulting discrete model for the Newton-Euler dynamics equations with Signorini's conditions is formulated as a LCP. For multi-rigid-body dynamic contact problems, Bar-

boteu and Dumont [40] have developed a PDAS type method to address the local treatment of the contact conditions using the Non-Smooth Contact Dynamics (NSCD) formalism [5, 6, 8, 41, 42]. Comparisons with the well-established methods bi-potential and augmented Lagrangian outline the efficiency of the NSCD-PDAS methods for the considered validation tests [40], dealing with frictionless model of muti-rigid-bodies contacts. The noted efficiency in [40] must be confirmed for problems involving friction. This contribution aims to provide a generalization of the NSCD-PDAS for dynamic frictional contact problems and to assess its efficiency with respect to the bi-potential and augmented Lagrangian theories.

The article is organized as follows. First, the mathematical model for the frictional contact conditions as formulated in contact dynamics is stated in Sec. 2. The complementary functions for both contact and friction are formulated in Sec. 3. In addition, their generalized derivatives are derived to provide the core of the Semi-Smooth Newton method. Section 4 presents the NSCD framework, especially the equations of motion, the local-global mapping and the NLGS iterative solver. Based on these prerequisites, Sec. 3 introduces two versions of the PDAS to tackle the frictional contact for solid rigid bodies. Several numerical experiments are reported in Sec. 6 for algorithm validation purposes and also to assess the efficiency and performances of PDAS methods with respect to the Newton/Augmented Lagrangian and the Bi-Potential methods. Finally, some perspectives and future works are presented in Sec. 7.

2. Frictional Contact conditions for Contact Dynamics

Let us consider, for the rest of this paper, a dynamic collection of rigid bodies involved in several simultaneous contacts. We focus exclusively on unilateral contact and dry friction interactions. In order to ensure reliable dynamics of such systems, one have to take into account the energy conservation properties. Hence, the choice of the contact model in the context of Non-Smooth Contact Dynamics (NSCD) depends on whether the nature of the physics to deal with is a collection of rigid bodies or not. On the assumption that a multi-rigid body system is concerned, the contact conditions are formulated in terms of velocity, unlike deformable bodies (cf [34, 35]), relating thus the impulse forces to the velocities. Then, the issue is to predict the velocities of the bodies and the impulse forces acting on the simultaneous multi-contacts.

Denoting by α a potential contact between two rigid particles of our system (α being a contact of the set of contact nodes $\mathcal{S}$), we recall in detail the unilateral contact with friction within the framework of rigid bodies. For that purpose, and for the sake of conciseness, we denote by $\boldsymbol{n}$ the unit inner normal vector from a particle to another and $\boldsymbol{\tau}$ the associated tangent vector. We use the notation $\boldsymbol{u}$ and $\boldsymbol{p}$ for the local displacement and the local impulse tensor at the contact point α, respectively (a dot superscript represents the time derivative with respect to the time variable t, e.g. $\dot{u} = \partial u/\partial t$). Also, we denote by $\dot{u}_n$ and $\dot{\boldsymbol{u}}_{\boldsymbol{\tau}}$ the normal and tangential components of velocity $\dot{\boldsymbol{u}}$ given by $\dot{u}_n = \dot{\boldsymbol{u}} \cdot \boldsymbol{n}$, $\dot{\boldsymbol{u}}_{\boldsymbol{\tau}} = \dot{\boldsymbol{u}} - u_n \boldsymbol{n}$. Finally, p_n and $\boldsymbol{p}_{\boldsymbol{\tau}}$ will represent the normal and the tangential impulse forces on the contact point, defined by $p_n = (\boldsymbol{p} \cdot \boldsymbol{n})\boldsymbol{n}$ and $\boldsymbol{p}_{\boldsymbol{\tau}} = \boldsymbol{p} - p_n \boldsymbol{n}$.

First, as long as the normal distance u_n between the two particles (corresponding to a gap) remains positive, there is no impulse force acting on each particle, and therefore, the normal impulse force p_n remains zero. When the gap $u_n = 0$, a repulsive normal impulse force p_n is mobilized at the contact point and it can take indefinitely large values depending on the forces acting on each particle. Furthermore, as we consider an unilateral contact with dry friction, the discrete conditions on the contact point with friction define two complementary relations, the first one called Signorini's conditions [43], between the normal velocity $\dot{u}_n$ and the normal impulse force p_n, and the second one called Coulomb's conditions [44], relating the tangential component of velocity $\dot{\boldsymbol{u}}_{\boldsymbol{\tau}}$ and the tangential

component of impulse force $\boldsymbol{p_\tau}$. The inelastic shock law's conditions can be written as follows:

$$\text{if} \quad g^\alpha > 0 \quad \text{then} \quad p_n^\alpha = 0, \tag{2.1}$$

$$\text{if} \quad g^\alpha \leq 0 \quad \text{then}$$

$$\dot{u}_n^\alpha \geq 0, \tag{2.2}$$

$$p_n^\alpha \geq 0, \tag{2.3}$$

$$\dot{u}_n^\alpha p_n^\alpha = 0, \tag{2.4}$$

where g^α is the signed distance between the particles (the gap). Relations (2.1) – (2.4) lead to the conditions of a complete contact law formulated by Moreau (see [5], [8]). The last condition (2.4), is a complementary relation that ensures impenetrability between bodies (see [2] for more details). On the other hand, for energy conservation purposes, (2.4), also called persistency condition, means that normal contact reaction only appear during persistent contact, and has to be added in order to vanish the work of normal contact impulses at time t and preserve the amount of energy before and after the shock. J.-J. Moreau has proven that these conditions ensure impenetrability between bodies; see J.-J. Moreau viability lemma (cf [5], [8]).

The Coulomb's friction law reads as,

$$\boldsymbol{p_\tau^\alpha} \neq \boldsymbol{0}. \tag{2.5}$$

$$\begin{cases} p_n^\alpha = 0 \Longrightarrow \dot{u}_n^\alpha \geq 0, \\ p_n^\alpha > 0 \quad and \quad ||\boldsymbol{p_\tau^\alpha}|| < \mu p_n^\alpha \Longrightarrow \boldsymbol{\dot{u}_\tau^\alpha} = 0, \\ p_n^\alpha > 0 \quad and \quad |\boldsymbol{p_\tau^\alpha}|| = \mu p_n^\alpha \Longrightarrow \exists \beta \geq 0, \boldsymbol{\dot{u}_\tau^\alpha} = \beta \frac{\boldsymbol{p_\tau^\alpha}}{||\boldsymbol{p_\tau^\alpha}||}. \end{cases} \tag{2.6}$$

where μ is the friction coefficient.

The non-smooth motion in the event of a collision implies velocity jumps. These velocity jumps are the result of the velocity formulation of the non-inter-penetrability condition. The time derivative $\dot{u}$ is not unique and then, the left-limit velocity $\dot{u}_n^-$ and the right-limit velocity $\dot{u}_n^+$ have to be distinguished. By analogy with a binary collision between two rigid particles, one can compute the right-limit velocity $\dot{u}_n^+$ on the basis of the left-limit one just before the contact in a time-stepping scheme. Thus, the computation of $\dot{u}_n$ involved in Signorini's conditions is motivated by a simple choice which requires the use of a weighted average between $\dot{u}_n^-$ and $\dot{u}_n^+$:
$\dot{u}_n = \eta \dot{u}_n^- + (1-\eta)\dot{u}_n^+$, where η is a material parameter characterizing the contact (for more details about the computation of $\dot{u}_n$, see [3]). Then, for $\eta \neq 0$, a binary shock between two rigid particles involves $\frac{-\dot{u}_n^+}{\dot{u}_n^-} = \frac{\eta}{(1-\eta)}$. By identifying this ratio with normal restitution coefficient of the material, we obtain $\eta = \frac{e_n}{(1+e_n)}$. Therefore, we define:

$$\dot{u}_n = \frac{\dot{u}_n^+ + e_n \dot{u}_n^-}{(1+e_n)} \tag{2.7}$$

Identically, the computation of the tangential velocity $\boldsymbol{\dot{u}}_n$ related to the frictional Coulomb's conditions follows the same way. The tangential impulse force $\boldsymbol{p_\tau}$ represents the average effect of static and repulsive forces relative to the contact during the time lapse Δt. The tangential velocity is then an average velocity (see [3]). By the same token as normal impulse forces, a simple consistent model with the tangential restitution coefficient is to define $\boldsymbol{\dot{u}_\tau}$ as follows:

$$\boldsymbol{\dot{u}_\tau} = \frac{\boldsymbol{\dot{u}_\tau^+} + e_{\boldsymbol{\tau}} \boldsymbol{\dot{u}_\tau^-}}{(1+e_{\boldsymbol{\tau}})} \tag{2.8}$$

In the following, two couples $(\dot{u}_n^\alpha, p_n^\alpha)$ and $(\tilde{\boldsymbol{\dot{u}}}^\alpha, \boldsymbol{p}^\alpha)$ verifying these set of conditions for a potential

contact node α between two particles are denoted by

$$\begin{cases} contact\_law(\dot{u}_n^\alpha, p_n^\alpha) = .true. \\ friction\_law(\tilde{\dot{\boldsymbol{u}}}^\alpha, \boldsymbol{p}^\alpha) = .true. \end{cases} \tag{2.9}$$

where $contact\_law(\dot{u}_n^\alpha, p_n^\alpha)$ is related to the the inelastic shock law's condtions ((2.1) – (2.4)), while $friction\_law(\tilde{\dot{\boldsymbol{u}}}^\alpha, \boldsymbol{p}^\alpha)$ describes the Coulomb's friction law ((2.5) – (2.6)).

3. Semi-Smooth Newton approach

3.1. Complementary function for the contact

The discrete Signorini's conditions (2.2)–(2.4) are represented by the following non-linear complementary function $\mathcal{C}_n^{\boldsymbol{p}}(\dot{u}_n^\alpha, p_n^\alpha) = 0$

$$\mathcal{C}_n^{\boldsymbol{p}}(\dot{u}_n^\alpha, p_n^\alpha) = p_n^\alpha - [p_n^\alpha - \gamma_n \dot{u}_n^\alpha]_+ \quad \forall \alpha \in \mathcal{S}, \tag{3.1}$$

where $\mathcal{S}$ is the set of all potential contact nodes, and γ_n the normal Active Set parameter. Now, let us prove this result.

Proposition 3.1. *Let $\gamma_n > 0$, the unilateral contact conditions expressed in velocity (2.2)–(2.4) for each potential contact α of the set of nodes $\mathcal{S}$ are equivalent to $\mathcal{C}_n^{\boldsymbol{p}}(\dot{u}_n^\alpha, p_n^\alpha) = 0$, where p_n^α is the normal impulse force between two particles in contact.*

Proof. Let us assume that (2.2)–(2.4) hold. We consider successively the cases $\dot{u}_n^\alpha > 0$ and $\dot{u}_n^\alpha = 0$. First, if $\dot{u}_n^\alpha > 0$, the condition $\dot{u}_n^\alpha p_n^\alpha = 0$ implies that $p_n^\alpha = 0$. Thus,

$$\mathcal{C}_n^{\boldsymbol{p}}(\dot{u}_n^\alpha, p_n^\alpha) = -[-\gamma_n \dot{u}_n^\alpha]_+ = 0,$$

since $\gamma_n > 0$. We suppose now that $\dot{u}_n^\alpha = 0$ and $p_n^\alpha > 0$; therefore

$$\mathcal{C}_n^{\boldsymbol{p}}(\dot{u}_n^\alpha, p_n^\alpha) = p_n^\alpha - [p_n^\alpha]_+ = 0.$$

Conversely, we assume now that $\mathcal{C}_n^{\boldsymbol{p}}(\dot{u}_n^\alpha, p_n^\alpha) = 0$ holds; it implies that $p_n^\alpha \geq 0$. Next, if $p_n^\alpha = 0$, we have

$$\mathcal{C}_n^{\boldsymbol{p}}(\dot{u}_n^\alpha, p_n^\alpha) = -[-\gamma_n \dot{u}_n^\alpha]_+ = 0,$$

which leads to $\dot{u}_n^\alpha \geq 0$, since $\gamma_n > 0$. Finally, if $p_n^\alpha > 0$, we have

$$\mathcal{C}_n^{\boldsymbol{p}}(\dot{u}_n^\alpha, p_n^\alpha) = p_n^\alpha - [p_n^\alpha - \gamma_n \dot{u}_n^\alpha]_+ = 0 \implies p_n^\alpha = p_n^\alpha - \gamma_n \dot{u}_n^\alpha$$

and since $\gamma_n > 0$, it implies that $\dot{u}_n^\alpha = 0$, which concludes the proof. A similar proof is available in [40]. □

3.2. Complementary function for the friction

The frictional Coulomb's conditions (2.6) are represented by the following non-linear complementary function $\mathcal{C}_{\boldsymbol{\tau}}^{\boldsymbol{p}}(\dot{u}_n^\alpha, \dot{\boldsymbol{u}}_{\boldsymbol{\tau}}^\alpha, p_n^\alpha, \boldsymbol{p}_{\boldsymbol{\tau}}^\alpha) = 0$

$$\mathcal{C}_{\boldsymbol{\tau}}^{\boldsymbol{p}}(\dot{u}_n^\alpha, \dot{\boldsymbol{u}}_{\boldsymbol{\tau}}^\alpha, p_n^\alpha, \boldsymbol{p}_{\boldsymbol{\tau}}^\alpha) = \max\left(\mu p_n^\alpha, ||\boldsymbol{p}_{\boldsymbol{\tau}}^\alpha - \gamma_{\boldsymbol{\tau}} \dot{\boldsymbol{u}}_{\boldsymbol{\tau}}^\alpha||\right) \boldsymbol{p}_{\boldsymbol{\tau}}^\alpha - \mu p_n^\alpha (\boldsymbol{p}_{\boldsymbol{\tau}}^\alpha - \gamma_{\boldsymbol{\tau}} \dot{\boldsymbol{u}}_{\boldsymbol{\tau}}^\alpha) \quad \forall \alpha \in \mathcal{S}, \tag{3.2}$$

where $\mathcal{S}$ is the set of all potential contact nodes, and $\gamma_{\boldsymbol{\tau}}$ the tangential Active Set parameter. Now, let us prove this result.

Proposition 3.2. *let $\gamma_{\boldsymbol{\tau}} > 0$, the frictional contact conditions expressed in velocity (2.6) for each contact α of the set of nodes $\mathcal{S}$ are equivalent to $\mathcal{C}_{\boldsymbol{\tau}}^{\boldsymbol{p}}(\dot{u}_n^\alpha, \dot{\boldsymbol{u}}_{\boldsymbol{\tau}}^\alpha, p_n^\alpha, \boldsymbol{p}_{\boldsymbol{\tau}}^\alpha) = 0$, where $\boldsymbol{p}_{\boldsymbol{\tau}}^\alpha$ is the tangential impulse force between two particles in contact.*

Proof. Let us assume that (2.6) hold. We consider successively the cases $p_n^\alpha = 0$ and $p_n^\alpha > 0$. First, if $p_n^\alpha = 0$, it implies that $\dot{u}_n^\alpha \geq 0$, and thus,

$$\mathcal{C}_{\boldsymbol{\tau}}^{\boldsymbol{p}}(\dot{u}_n^\alpha, \dot{\boldsymbol{u}}_{\boldsymbol{\tau}}^\alpha, p_n^\alpha, \boldsymbol{p}_{\boldsymbol{\tau}}^\alpha) = ||\boldsymbol{p}_{\boldsymbol{\tau}}^\alpha - \gamma_{\boldsymbol{\tau}} \dot{\boldsymbol{u}}_{\boldsymbol{\tau}}^\alpha|| \boldsymbol{p}_{\boldsymbol{\tau}}^\alpha,$$

Since there is no contact, $\boldsymbol{p}_{\boldsymbol{\tau}}^\alpha = 0$. Finally, $\mathcal{C}_{\boldsymbol{\tau}}^{\boldsymbol{p}}(\dot{u}_n^\alpha, \dot{\boldsymbol{u}}_{\boldsymbol{\tau}}^\alpha, p_n^\alpha, \boldsymbol{p}_{\boldsymbol{\tau}}^\alpha) = 0$.

We suppose now that $p_n^\alpha > 0$ and $||\boldsymbol{p}_{\boldsymbol{\tau}}^\alpha|| < \mu p_n^\alpha$; it implies that $\dot{\boldsymbol{u}}_{\boldsymbol{\tau}}^\alpha = 0$. Therefore, and since $\gamma_{\boldsymbol{\tau}} > 0$, we have

$$\mathcal{C}_{\boldsymbol{\tau}}^{\boldsymbol{p}}(\dot{u}_n^\alpha, \dot{\boldsymbol{u}}_{\boldsymbol{\tau}}^\alpha, p_n^\alpha, \boldsymbol{p}_{\boldsymbol{\tau}}^\alpha) = \max\left(\mu p_n^\alpha, ||\boldsymbol{p}_{\boldsymbol{\tau}}^\alpha||\right) \boldsymbol{p}_{\boldsymbol{\tau}}^\alpha - \mu p_n^\alpha \boldsymbol{p}_{\boldsymbol{\tau}}^\alpha,$$

Then,

$$\mathcal{C}_{\boldsymbol{\tau}}^{\boldsymbol{p}}(\dot{u}_n^\alpha, \dot{\boldsymbol{u}}_{\boldsymbol{\tau}}^\alpha, p_n^\alpha, \boldsymbol{p}_{\boldsymbol{\tau}}^\alpha) = \mu p_n^\alpha \boldsymbol{p}_{\boldsymbol{\tau}}^\alpha - \mu p_n^\alpha \boldsymbol{p}_{\boldsymbol{\tau}}^\alpha = 0.$$

We suppose now that $p_n^\alpha > 0$, $||\boldsymbol{p}_{\boldsymbol{\tau}}^\alpha|| = \mu p_n^\alpha$ and $\dot{\boldsymbol{u}}_{\boldsymbol{\tau}}^{\boldsymbol{\alpha}} = \beta \frac{\boldsymbol{p}_{\boldsymbol{\tau}}^\alpha}{||\boldsymbol{p}_{\boldsymbol{\tau}}^\alpha||}$ with $\beta \geq 0$; therefore

$$\mathcal{C}_{\boldsymbol{\tau}}^{\boldsymbol{p}}(\dot{u}_n^\alpha, \dot{\boldsymbol{u}}_{\boldsymbol{\tau}}^\alpha, p_n^\alpha, \boldsymbol{p}_{\boldsymbol{\tau}}^\alpha) = \max\left(\mu p_n^\alpha, ||\boldsymbol{p}_{\boldsymbol{\tau}}^\alpha - \gamma_{\boldsymbol{\tau}} \beta \frac{\boldsymbol{p}_{\boldsymbol{\tau}}^\alpha}{||\mu p_n^\alpha||}||\right) \boldsymbol{p}_{\boldsymbol{\tau}}^\alpha - \mu p_n^\alpha (\boldsymbol{p}_{\boldsymbol{\tau}}^\alpha - \gamma_{\boldsymbol{\tau}} \beta \frac{\boldsymbol{p}_{\boldsymbol{\tau}}^\alpha}{||\mu p_n^\alpha||}) = 0.$$

Conversely, we assume now that $\mathcal{C}_{\boldsymbol{\tau}}^{\boldsymbol{p}}(\dot{u}_n^\alpha, \dot{\boldsymbol{u}}_{\boldsymbol{\tau}}^\alpha, p_n^\alpha, \boldsymbol{p}_{\boldsymbol{\tau}}^\alpha) = 0$ holds; depending on the value of $\boldsymbol{p}_{\boldsymbol{\tau}}^\alpha$ and $\dot{\boldsymbol{u}}_{\boldsymbol{\tau}}^\alpha$, one can have

$$\mu p_n^\alpha = \max\left(\mu p_n^\alpha, ||\boldsymbol{p}_{\boldsymbol{\tau}}^\alpha - \gamma_{\boldsymbol{\tau}} \dot{\boldsymbol{u}}_{\boldsymbol{\tau}}^\alpha||\right), \tag{3.3}$$

$$||\boldsymbol{p}_{\boldsymbol{\tau}}^\alpha - \gamma_{\boldsymbol{\tau}} \dot{\boldsymbol{u}}_{\boldsymbol{\tau}}^\alpha|| = \max\left(\mu p_n^\alpha, ||\boldsymbol{p}_{\boldsymbol{\tau}}^\alpha - \gamma_{\boldsymbol{\tau}} \dot{\boldsymbol{u}}_{\boldsymbol{\tau}}^\alpha||\right), \tag{3.4}$$

By combining (3.2) and (3.3), we get

$$\mu p_n^\alpha \boldsymbol{p}_{\boldsymbol{\tau}}^\alpha - \mu p_n^\alpha \boldsymbol{p}_{\boldsymbol{\tau}}^\alpha + \mu \gamma_{\boldsymbol{\tau}} p_n^\alpha \dot{\boldsymbol{u}}_{\boldsymbol{\tau}}^\alpha = 0,$$

which means that $p_n^\alpha \dot{\boldsymbol{u}}_{\boldsymbol{\tau}}^\alpha = 0$, since $\gamma_n > 0$ and $\mu > 0$. If $p_n^\alpha = 0$, condition (2.4) implies that $\dot{u}_n^\alpha \geq 0$. If not, $p_n^\alpha > 0$, $\dot{\boldsymbol{u}}_{\boldsymbol{\tau}}^\alpha = 0$ and from (3.3), $\mu p_n^\alpha > ||\boldsymbol{p}_{\boldsymbol{\tau}}^\alpha||$.
At last, we combine (3.2) and (3.4) to obtain

$$||\boldsymbol{p}_{\boldsymbol{\tau}}^\alpha - \gamma_{\boldsymbol{\tau}} \dot{\boldsymbol{u}}_{\boldsymbol{\tau}}^\alpha|| \boldsymbol{p}_{\boldsymbol{\tau}}^\alpha - \mu p_n^\alpha \boldsymbol{p}_{\boldsymbol{\tau}}^\alpha + \mu \gamma_{\boldsymbol{\tau}} p_n^\alpha \dot{\boldsymbol{u}}_{\boldsymbol{\tau}}^\alpha = 0.$$

It is trivial that

$$\boldsymbol{p}_{\boldsymbol{\tau}}^\alpha = \frac{\mu \gamma_{\boldsymbol{\tau}} p_n^\alpha}{\mu p_n^\alpha - ||\boldsymbol{p}_{\boldsymbol{\tau}}^\alpha - \gamma_{\boldsymbol{\tau}} \dot{\boldsymbol{u}}_{\boldsymbol{\tau}}^\alpha||} \dot{\boldsymbol{u}}_{\boldsymbol{\tau}}^\alpha,$$

let $\beta = \frac{\mu \gamma_{\boldsymbol{\tau}} p_n^\alpha}{\mu p_n^\alpha - ||\boldsymbol{p}_{\boldsymbol{\tau}}^\alpha - \gamma_{\boldsymbol{\tau}} \dot{\boldsymbol{u}}_{\boldsymbol{\tau}}^\alpha||}$. If $p_n^\alpha > 0$ and $||\boldsymbol{p}_{\boldsymbol{\tau}}^\alpha|| = \mu p_n^\alpha$, and implies that $\dot{u}_n^\alpha > 0$, since $\gamma_n > 0$, which concludes the proof. □

3.3. Generalized derivative of complementary functions

Now, we provide the generalized derivative of the complementary functions in the gap, stick and slip cases.

- Gap case : $p_n^\alpha - \gamma_n \dot{u}_n^\alpha \leq 0$

According to the complementary functions $\mathcal{C}_n^{\boldsymbol{p}}(\dot{u}_n^\alpha, p_n^\alpha) = p_n^\alpha$ and $\mathcal{C}_{\boldsymbol{\tau}}^{\boldsymbol{p}}(\dot{u}_n^\alpha, \dot{\boldsymbol{u}}_{\boldsymbol{\tau}}^\alpha, p_n^\alpha, \boldsymbol{p}_{\boldsymbol{\tau}}^\alpha) = \|\boldsymbol{p}_{\boldsymbol{\tau}}^\alpha - \gamma_{\boldsymbol{\tau}} \dot{\boldsymbol{u}}_{\boldsymbol{\tau}}^\alpha\| \boldsymbol{p}_{\boldsymbol{\tau}}^\alpha$, we have the following derivatives

$$d_{\dot{u}_n^\alpha} \mathcal{C}_n^{\boldsymbol{p}} = 0, \tag{3.5}$$

$$d_{p_n^\alpha} \mathcal{C}_n^{\boldsymbol{p}} = dp_n^\alpha, \tag{3.6}$$

$$d_{\dot{u}_n^\alpha} \mathcal{C}_{\boldsymbol{\tau}}^{\boldsymbol{p}} = 0, \tag{3.7}$$

$$d_{\dot{\boldsymbol{u}}_{\boldsymbol{\tau}}^\alpha} \mathcal{C}_{\boldsymbol{\tau}}^{\boldsymbol{p}} = -\gamma_{\boldsymbol{\tau}} \boldsymbol{p}_{\boldsymbol{\tau}}^\alpha \frac{(\boldsymbol{p}_{\boldsymbol{\tau}}^\alpha - \gamma_{\boldsymbol{\tau}} \dot{\boldsymbol{u}}_{\boldsymbol{\tau}}^\alpha)^T}{\|\boldsymbol{p}_{\boldsymbol{\tau}}^\alpha - \gamma_{\boldsymbol{\tau}} \dot{\boldsymbol{u}}_{\boldsymbol{\tau}}^\alpha\|} d\dot{\boldsymbol{u}}_{\boldsymbol{\tau}}^\alpha = 0, \tag{3.8}$$

$$d_{p_n^\alpha} \mathcal{C}_{\boldsymbol{\tau}}^{\boldsymbol{p}} = 0, \tag{3.9}$$

$$d_{\boldsymbol{p}_{\boldsymbol{\tau}}^\alpha} \mathcal{C}_{\boldsymbol{\tau}}^{\boldsymbol{p}} = \Big(\boldsymbol{p}_{\boldsymbol{\tau}}^\alpha \frac{(\boldsymbol{p}_{\boldsymbol{\tau}}^\alpha - \gamma_{\boldsymbol{\tau}} \dot{\boldsymbol{u}}_{\boldsymbol{\tau}}^\alpha)^T}{\|\boldsymbol{p}_{\boldsymbol{\tau}}^\alpha - \gamma_{\boldsymbol{\tau}} \dot{\boldsymbol{u}}_{\boldsymbol{\tau}}^\alpha\|} + \|\boldsymbol{p}_{\boldsymbol{\tau}}^\alpha - \gamma_{\boldsymbol{\tau}} \dot{\boldsymbol{u}}_{\boldsymbol{\tau}}^\alpha\| \boldsymbol{I}_2 \Big) d\boldsymbol{p}_{\boldsymbol{\tau}}^\alpha. \tag{3.10}$$

- Stick case : $\mu p_n^\alpha \geq \|\boldsymbol{p}_{\boldsymbol{\tau}}^\alpha - \gamma_{\boldsymbol{\tau}} \dot{\boldsymbol{u}}_{\boldsymbol{\tau}}^\alpha\| > 0$

Given the complementary functions $\mathcal{C}_n^{\boldsymbol{p}}(\dot{u}_n^\alpha, p_n^\alpha) = \gamma_n \dot{u}_n^\alpha$ and $\mathcal{C}_{\boldsymbol{\tau}}^{\boldsymbol{p}}(\dot{u}_n^\alpha, \dot{\boldsymbol{u}}_{\boldsymbol{\tau}}^\alpha, p_n^\alpha, \boldsymbol{p}_{\boldsymbol{\tau}}^\alpha) = \mu\gamma_{\boldsymbol{\tau}} p_n^\alpha \dot{\boldsymbol{u}}_{\boldsymbol{\tau}}^\alpha$, we have

$$d_{\dot{u}_n^\alpha}\mathcal{C}_n^{\boldsymbol{p}} = \gamma_n d\dot{u}_n^\alpha, \tag{3.11}$$
$$d_{p_n^\alpha}\mathcal{C}_n^{\boldsymbol{p}} = 0, \tag{3.12}$$
$$d_{\dot{u}_n^\alpha}\mathcal{C}_{\boldsymbol{\tau}}^{\boldsymbol{p}} = 0, \tag{3.13}$$
$$d_{\dot{\boldsymbol{u}}_{\boldsymbol{\tau}}^\alpha}\mathcal{C}_{\boldsymbol{\tau}}^{\boldsymbol{p}} = \mu\gamma_{\boldsymbol{\tau}} p_n^\alpha d\dot{\boldsymbol{u}}_{\boldsymbol{\tau}}^\alpha, \tag{3.14}$$
$$d_{p_n^\alpha}\mathcal{C}_{\boldsymbol{\tau}}^{\boldsymbol{p}} = \mu\gamma_{\boldsymbol{\tau}} \dot{\boldsymbol{u}}_{\boldsymbol{\tau}}^\alpha dp_n^\alpha, \tag{3.15}$$
$$d_{\boldsymbol{p}_{\boldsymbol{\tau}}^\alpha}\mathcal{C}_{\boldsymbol{\tau}}^{\boldsymbol{p}} = 0. \tag{3.16}$$

- Slip case : $\|\boldsymbol{p}_{\boldsymbol{\tau}}^\alpha - \gamma_{\boldsymbol{\tau}} \dot{\boldsymbol{u}}_{\boldsymbol{\tau}}^\alpha\| > \mu p_n^\alpha > 0$

From $\mathcal{C}_n^{\boldsymbol{p}}(\dot{u}_n^\alpha, p_n^\alpha) = \gamma_n \dot{u}_n^\alpha$ and $\mathcal{C}_{\boldsymbol{\tau}}^{\boldsymbol{p}}(\dot{u}_n^\alpha, \dot{\boldsymbol{u}}_{\boldsymbol{\tau}}^\alpha, p_n^\alpha, \boldsymbol{p}_{\boldsymbol{\tau}}^\alpha) = \|\boldsymbol{p}_{\boldsymbol{\tau}}^\alpha - \gamma_{\boldsymbol{\tau}} \dot{\boldsymbol{u}}_{\boldsymbol{\tau}}^\alpha\| \boldsymbol{p}_{\boldsymbol{\tau}}^\alpha - \mu p_n^\alpha (\boldsymbol{p}_{\boldsymbol{\tau}}^\alpha - \gamma_{\boldsymbol{\tau}} \dot{\boldsymbol{u}}_{\boldsymbol{\tau}}^\alpha)$, it comes

$$d_{\dot{u}_n^\alpha}\mathcal{C}_n^{\boldsymbol{p}} = \gamma_n d\dot{u}_n^\alpha, \tag{3.17}$$
$$d_{p_n^\alpha}\mathcal{C}_n^{\boldsymbol{p}} = 0, \tag{3.18}$$
$$d_{\dot{u}_n^\alpha}\mathcal{C}_{\boldsymbol{\tau}}^{\boldsymbol{p}} = 0, \tag{3.19}$$
$$d_{\dot{\boldsymbol{u}}_{\boldsymbol{\tau}}^\alpha}\mathcal{C}_{\boldsymbol{\tau}}^{\boldsymbol{p}} = \Big(- \gamma_{\boldsymbol{\tau}} \boldsymbol{p}_{\boldsymbol{\tau}}^\alpha \frac{(\boldsymbol{p}_{\boldsymbol{\tau}}^\alpha - \gamma_{\boldsymbol{\tau}} \dot{\boldsymbol{u}}_{\boldsymbol{\tau}}^\alpha)^T}{\|\boldsymbol{p}_{\boldsymbol{\tau}}^\alpha - \gamma_{\boldsymbol{\tau}} \dot{\boldsymbol{u}}_{\boldsymbol{\tau}}^\alpha\|} + \mu\gamma_{\boldsymbol{\tau}} p_n^\alpha \boldsymbol{I}_2 \Big) d\dot{\boldsymbol{u}}_{\boldsymbol{\tau}}^\alpha, \tag{3.20}$$
$$d_{p_n^\alpha}\mathcal{C}_{\boldsymbol{\tau}}^{\boldsymbol{p}} = -\mu(\boldsymbol{p}_{\boldsymbol{\tau}}^\alpha - \gamma_{\boldsymbol{\tau}} \dot{\boldsymbol{u}}_{\boldsymbol{\tau}}^\alpha) dp_n^\alpha, \tag{3.21}$$
$$d_{\boldsymbol{p}_{\boldsymbol{\tau}}^\alpha}\mathcal{C}_{\boldsymbol{\tau}}^{\boldsymbol{p}} = \Big(\boldsymbol{p}_{\boldsymbol{\tau}}^\alpha \frac{(\boldsymbol{p}_{\boldsymbol{\tau}}^\alpha - \gamma_{\boldsymbol{\tau}} \dot{\boldsymbol{u}}_{\boldsymbol{\tau}}^\alpha)^T}{\|\boldsymbol{p}_{\boldsymbol{\tau}}^\alpha - \gamma_{\boldsymbol{\tau}} \dot{\boldsymbol{u}}_{\boldsymbol{\tau}}^\alpha\|} + \|\boldsymbol{p}_{\boldsymbol{\tau}}^\alpha - \gamma_{\boldsymbol{\tau}} \dot{\boldsymbol{u}}_{\boldsymbol{\tau}}^\alpha\| \boldsymbol{I}_2 - \mu p_n^\alpha \boldsymbol{I}_2 \Big) d\boldsymbol{p}_{\boldsymbol{\tau}}^\alpha. \tag{3.22}$$

By combining (3.5)–(3.22), with $\mathcal{D}_{\mathcal{C}_n^{\boldsymbol{p}}}$ and $\mathcal{D}_{\mathcal{C}_{\boldsymbol{\tau}}^{\boldsymbol{p}}}$ the generalized derivative of $\mathcal{C}_n^{\boldsymbol{p}}$ and $\mathcal{C}_{\boldsymbol{\tau}}^{\boldsymbol{p}}$, respectively, we obtain

$$\mathcal{D}_{\mathcal{C}_n^{\boldsymbol{p}}}(\dot{u}_n^\alpha, p_n^\alpha)(\delta\dot{u}_n^\alpha, \delta p_n^\alpha) = \gamma_n(1_{Stick} + 1_{Slip})\delta\dot{u}_n^\alpha + 1_{Gap}\delta p_n^\alpha, \tag{3.23}$$
$$\begin{aligned}\mathcal{D}_{\mathcal{C}_{\boldsymbol{\tau}}^{\boldsymbol{p}}}(\dot{u}_n^\alpha, \dot{\boldsymbol{u}}_{\boldsymbol{\tau}}^\alpha, p_n^\alpha, \boldsymbol{p}_{\boldsymbol{\tau}}^\alpha)(\delta\dot{u}_n^\alpha, \delta\dot{\boldsymbol{u}}_{\boldsymbol{\tau}}^\alpha, \delta p_n^\alpha, \delta\boldsymbol{p}_{\boldsymbol{\tau}}^\alpha) &= 1_{Gap}\|\boldsymbol{p}_{\boldsymbol{\tau}}^\alpha - \gamma_{\boldsymbol{\tau}} \dot{\boldsymbol{u}}_{\boldsymbol{\tau}}^\alpha\| \delta\boldsymbol{p}_{\boldsymbol{\tau}}^\alpha \\ &+ 1_{Stick}\Big(\mu\gamma_{\boldsymbol{\tau}} p_n^\alpha \delta\dot{\boldsymbol{u}}_{\boldsymbol{\tau}}^\alpha + \mu\gamma_{\boldsymbol{\tau}} \dot{\boldsymbol{u}}_{\boldsymbol{\tau}}^\alpha \delta p_n^\alpha\Big) \\ &+ 1_{Slip}\Big(\Big(- \gamma_{\boldsymbol{\tau}} \boldsymbol{p}_{\boldsymbol{\tau}}^\alpha \frac{(\boldsymbol{p}_{\boldsymbol{\tau}}^\alpha - \gamma_{\boldsymbol{\tau}} \dot{\boldsymbol{u}}_{\boldsymbol{\tau}}^\alpha)^T}{\|\boldsymbol{p}_{\boldsymbol{\tau}}^\alpha - \gamma_{\boldsymbol{\tau}} \dot{\boldsymbol{u}}_{\boldsymbol{\tau}}^\alpha\|} + \mu\gamma_{\boldsymbol{\tau}} p_n^\alpha \boldsymbol{I}_2\Big)\delta\dot{\boldsymbol{u}}_{\boldsymbol{\tau}}^\alpha - \mu(\boldsymbol{p}_{\boldsymbol{\tau}}^\alpha - \gamma_{\boldsymbol{\tau}} \dot{\boldsymbol{u}}_{\boldsymbol{\tau}}^\alpha)\delta p_n^\alpha \\ &+ \Big(\boldsymbol{p}_{\boldsymbol{\tau}}^\alpha \frac{(\boldsymbol{p}_{\boldsymbol{\tau}}^\alpha - \gamma_{\boldsymbol{\tau}} \dot{\boldsymbol{u}}_{\boldsymbol{\tau}}^\alpha)^T}{\|\boldsymbol{p}_{\boldsymbol{\tau}}^\alpha - \gamma_{\boldsymbol{\tau}} \dot{\boldsymbol{u}}_{\boldsymbol{\tau}}^\alpha\|} + \|\boldsymbol{p}_{\boldsymbol{\tau}}^\alpha - \gamma_{\boldsymbol{\tau}} \dot{\boldsymbol{u}}_{\boldsymbol{\tau}}^\alpha\| \boldsymbol{I}_2 - \mu p_n^\alpha \boldsymbol{I}_2\Big)\delta\boldsymbol{p}_{\boldsymbol{\tau}}^\alpha\Big)\end{aligned} \tag{3.24}$$

where

$$\begin{aligned}&1_{Gap} = 1, 1_{Stick} = 0, 1_{Slip} = 0 \text{ if } p_n^\alpha - \gamma_n \dot{u}_n^\alpha \leq 0, \\ &1_{Gap} = 0, 1_{Stick} = 1, 1_{Slip} = 0 \text{ if } \mu p_n^\alpha \geq \|\boldsymbol{p}_{\boldsymbol{\tau}}^\alpha - \gamma_{\boldsymbol{\tau}} \dot{\boldsymbol{u}}_{\boldsymbol{\tau}}^\alpha\| > 0, \\ &1_{Gap} = 0, 1_{Stick} = 0, 1_{Slip} = 1 \text{ if } \|\boldsymbol{p}_{\boldsymbol{\tau}}^\alpha - \gamma_{\boldsymbol{\tau}} \dot{\boldsymbol{u}}_{\boldsymbol{\tau}}^\alpha\| > \mu p_n^\alpha > 0.\end{aligned}$$

Using now the semi-smooth Newton formalism at the current $(\dot{u}_n^{\alpha,(k)}, \dot{\boldsymbol{u}}_{\boldsymbol{\tau}}^{\alpha,(k)}, p_n^{\alpha,(k)}, \boldsymbol{p}_{\boldsymbol{\tau}}^{\alpha,(k)})$, one can derive the new iterate $(\dot{u}_n^{\alpha,(k+1)}, \dot{\boldsymbol{u}}_{\boldsymbol{\tau}}^{\alpha,(k+1)}, p_n^{\alpha,(k+1)}, \boldsymbol{p}_{\boldsymbol{\tau}}^{\alpha,(k+1)})$

$$\mathcal{D}_{\mathcal{C}_n^{\boldsymbol{p}}}(\dot{u}_n^{\alpha,(k)}, p_n^{\alpha,(k)})(\delta\dot{u}_n^{\alpha,(k+1)}, \delta p_n^{\alpha,(k+1)}) = -\mathcal{C}_n^{\boldsymbol{p}}(\dot{u}_n^{\alpha,(k)}, p_n^{\alpha,(k)}), \tag{3.25}$$

$$\begin{aligned}&\mathcal{D}_{\mathcal{C}_{\boldsymbol{\tau}}^{\boldsymbol{p}}}(\dot{u}_n^{\alpha,(k)}, \dot{\boldsymbol{u}}_{\boldsymbol{\tau}}^{\alpha,(k)}, p_n^{\alpha,(k)}, \boldsymbol{p}_{\boldsymbol{\tau}}^{\alpha,(k)})(\delta\dot{u}_n^{\alpha,(k+1)}, \delta\dot{\boldsymbol{u}}_{\boldsymbol{\tau}}^{\alpha,(k+1)}, \delta p_n^{\alpha,(k+1)}, \delta\boldsymbol{p}_{\boldsymbol{\tau}}^{\alpha,(k+1)}) \\ &= -\mathcal{C}_{\boldsymbol{\tau}}^{\boldsymbol{p}}(\dot{u}_n^{\alpha,(k)}, \dot{\boldsymbol{u}}_{\boldsymbol{\tau}}^{\alpha,(k)}, p_n^{\alpha,(k)}, \boldsymbol{p}_{\boldsymbol{\tau}}^{\alpha,(k)}),\end{aligned} \tag{3.26}$$

$$\begin{aligned}&(\dot{u}_n^{\alpha,(k+1)}, \dot{\boldsymbol{u}}_{\boldsymbol{\tau}}^{\alpha,(k+1)}, p_n^{\alpha,(k+1)}, \boldsymbol{p}_{\boldsymbol{\tau}}^{\alpha,(k+1)}) \\ &= (\dot{u}_n^{\alpha,(k)}, \dot{\boldsymbol{u}}_{\boldsymbol{\tau}}^{\alpha,(k)}, p_n^{\alpha,(k)}, \boldsymbol{p}_{\boldsymbol{\tau}}^{\alpha,(k)}) + (\delta\dot{u}_n^{\alpha,(k+1)}, \delta\dot{\boldsymbol{u}}_{\boldsymbol{\tau}}^{\alpha,(k+1)}, \delta p_n^{\alpha,(k+1)}, \delta\boldsymbol{p}_{\boldsymbol{\tau}}^{\alpha,(k+1)}).\end{aligned} \tag{3.27}$$

- Gap case: $1_{Gap} = 1, 1_{Stick} = 0, 1_{Slip} = 0$

From the equations (3.25) and (3.26) we have

$$p_n^{\alpha,(k+1)} - p_n^{\alpha,(k)} = -p_n^{\alpha,(k)}, \tag{3.28}$$

$$\|\boldsymbol{p}_{\boldsymbol{\tau}}^{\alpha,(k)} - \gamma_{\boldsymbol{\tau}} \dot{\boldsymbol{u}}_{\boldsymbol{\tau}}^{\alpha,(k)}\|(\boldsymbol{p}_{\boldsymbol{\tau}}^{\alpha,(k+1)} - \boldsymbol{p}_{\boldsymbol{\tau}}^{\alpha,(k)}) = -\|\boldsymbol{p}_{\boldsymbol{\tau}}^{\alpha,(k)} - \gamma_{\boldsymbol{\tau}} \dot{\boldsymbol{u}}_{\boldsymbol{\tau}}^{\alpha,(k)}\|\boldsymbol{p}_{\boldsymbol{\tau}}^{\alpha,(k)}. \tag{3.29}$$

Next, the gap conditions of the semi-smooth Newton formalism are as follows

$$p_n^{\alpha,(k+1)} = 0, \tag{3.30}$$

$$\boldsymbol{p}_{\boldsymbol{\tau}}^{\alpha,(k+1)} = \boldsymbol{0}, \tag{3.31}$$

since $\|\boldsymbol{p}_{\boldsymbol{\tau}}^{\alpha,(k)} - \gamma_{\boldsymbol{\tau}} \dot{\boldsymbol{u}}_{\boldsymbol{\tau}}^{\alpha,(k)}\| > 0$.

- Stick case : $1_{Gap} = 0, 1_{Stick} = 1, 1_{Slip} = 0$

From the equations (3.25) and (3.26) we have

$$\gamma_n(\dot{u}_n^{\alpha,(k+1)} - \dot{u}_n^{\alpha,(k)}) = -\gamma_n \dot{u}_n^{\alpha,(k)}, \tag{3.32}$$

$$\mu\gamma_{\boldsymbol{\tau}} p_n^{\alpha,(k)}(\dot{\boldsymbol{u}}_{\boldsymbol{\tau}}^{\alpha,(k+1)} - \dot{\boldsymbol{u}}_{\boldsymbol{\tau}}^{\alpha,(k)}) + \mu\gamma_{\boldsymbol{\tau}} \dot{\boldsymbol{u}}_{\boldsymbol{\tau}}^{\alpha,(k)}(p_n^{\alpha,(k+1)} - p_n^{\alpha,(k)}) = -\mu\gamma_{\boldsymbol{\tau}} p_n^{\alpha,(k)} \dot{\boldsymbol{u}}_{\boldsymbol{\tau}}^{\alpha,(k)}. \tag{3.33}$$

Next,

$$\dot{u}_n^{\alpha,(k+1)} = 0, \tag{3.34}$$

$$\dot{\boldsymbol{u}}_{\boldsymbol{\tau}}^{\alpha,(k+1)} - \dot{\boldsymbol{u}}_{\boldsymbol{\tau}}^{\alpha,(k)} = -\dot{\boldsymbol{u}}_{\boldsymbol{\tau}}^{\alpha,(k)} \frac{p_n^{\alpha,(k+1)}}{p_n^{\alpha,(k)}}. \tag{3.35}$$

For a given contact node α, the fundamental principle of dynamics can be written as follows:

$$\dot{\boldsymbol{u}}^{\alpha} = \dot{\boldsymbol{u}}^{\alpha,free} + \mathcal{W}^{\alpha\alpha}\boldsymbol{p}^{\alpha} + \sum_{\beta \neq \alpha} \mathcal{W}^{\beta\alpha}\boldsymbol{p}^{\beta}, \tag{3.36}$$

then, from (3.27), we have

$$\begin{cases} \delta\dot{\boldsymbol{u}}^{\alpha,(k+1)} = \dot{\boldsymbol{u}}^{\alpha,(k+1)} - \dot{\boldsymbol{u}}^{\alpha,(k)}, \\ \delta\boldsymbol{p}^{\alpha,(k+1)} = \boldsymbol{p}^{\alpha,(k+1)} - \boldsymbol{p}^{\alpha,(k)}, \end{cases} \tag{3.37}$$

using (3.36), one can write

$$\delta\dot{\boldsymbol{u}}^{\alpha,(k+1)} = \mathcal{W}^{\alpha\alpha}\delta\boldsymbol{p}^{\alpha,(k+1)}, \tag{3.38}$$

and more particularly,

$$\delta\dot{\boldsymbol{u}}_{\boldsymbol{\tau}}^{\alpha,(k+1)} = \mathcal{W}_{\boldsymbol{\tau}\boldsymbol{\tau}}^{\alpha\alpha}\delta\boldsymbol{p}_{\boldsymbol{\tau}}^{\alpha,(k+1)}, \tag{3.39}$$

then,

$$\dot{\boldsymbol{u}}_{\boldsymbol{\tau}}^{\alpha,(k+1)} - \dot{\boldsymbol{u}}_{\boldsymbol{\tau}}^{\alpha,(k)} = \mathcal{W}_{\boldsymbol{\tau}\boldsymbol{\tau}}^{\alpha\alpha}(\boldsymbol{p}_{\boldsymbol{\tau}}^{\alpha,(k+1)} - \boldsymbol{p}_{\boldsymbol{\tau}}^{\alpha,(k)}). \tag{3.40}$$

By combining (3.35) and (3.40), we get

$$-\dot{\boldsymbol{u}}_{\boldsymbol{\tau}}^{\alpha,(k)} \frac{p_n^{\alpha,(k+1)}}{p_n^{\alpha,(k)}} = \mathcal{W}_{\boldsymbol{\tau}\boldsymbol{\tau}}^{\alpha\alpha}(\boldsymbol{p}_{\boldsymbol{\tau}}^{\alpha,(k+1)} - \boldsymbol{p}_{\boldsymbol{\tau}}^{\alpha,(k)}). \tag{3.41}$$

Finally, the stick conditions of the semi-smooth Newton formalism are as follows (in the case of a diagonal matrix $\mathcal{W}_{\boldsymbol{\tau}\boldsymbol{\tau}}^{\alpha\alpha}$)

$$\dot{u}_n^{\alpha,(k+1)} = 0, \tag{3.42}$$

$$\boldsymbol{p}_{\boldsymbol{\tau}}^{\alpha,(k+1)} + \frac{\frac{p_n^{\alpha,(k+1)}}{p_n^{\alpha,(k)}}\dot{\boldsymbol{u}}_{\boldsymbol{\tau}}^{\alpha,(k)}}{\mathcal{W}_{\boldsymbol{\tau}\boldsymbol{\tau}}^{\alpha\alpha}} = \boldsymbol{p}_{\boldsymbol{\tau}}^{\alpha,(k)}. \tag{3.43}$$

- Slip case: $1_{Gap} = 0, 1_{Stick} = 0, 1_{Slip} = 1$

For $\mathcal{C}_n^{\boldsymbol{p}}$, we get once again

$$\dot{u}_n^{\alpha,(k+1)} = 0. \tag{3.44}$$

For $\mathcal{C}_{\boldsymbol{\tau}}^{\boldsymbol{p}}$, we obtain

$$\begin{aligned}
&\Big(- \gamma_{\boldsymbol{\tau}} \boldsymbol{p}_{\boldsymbol{\tau}}^{\alpha,(k)} \frac{(\boldsymbol{p}_{\boldsymbol{\tau}}^{\alpha,(k)} - \gamma_{\boldsymbol{\tau}}\dot{\boldsymbol{u}}_{\boldsymbol{\tau}}^{\alpha,(k)})^T}{\|\boldsymbol{p}_{\boldsymbol{\tau}}^{\alpha,(k)} - \gamma_{\boldsymbol{\tau}}\dot{\boldsymbol{u}}_{\boldsymbol{\tau}}^{\alpha,(k)}\|} + \mu\gamma_{\boldsymbol{\tau}} p_n^{\alpha,(k)} \boldsymbol{I}_2\Big)(\dot{\boldsymbol{u}}_{\boldsymbol{\tau}}^{\alpha,(k+1)} - \dot{\boldsymbol{u}}_{\boldsymbol{\tau}}^{\alpha,(k)}) \\
&- \mu(\boldsymbol{p}_{\boldsymbol{\tau}}^{\alpha,(k)} - \gamma_{\boldsymbol{\tau}}\dot{\boldsymbol{u}}_{\boldsymbol{\tau}}^{\alpha,(k)})(p_n^{\alpha,(k+1)} - p_n^{\alpha,(k)}) \\
&+ \Big(\boldsymbol{p}_{\boldsymbol{\tau}}^{\alpha,(k)} \frac{(\boldsymbol{p}_{\boldsymbol{\tau}}^{\alpha,(k)} - \gamma_{\boldsymbol{\tau}}\dot{\boldsymbol{u}}_{\boldsymbol{\tau}}^{\alpha,(k)})^T}{\|\boldsymbol{p}_{\boldsymbol{\tau}}^{\alpha,(k)} - \gamma_{\boldsymbol{\tau}}\dot{\boldsymbol{u}}_{\boldsymbol{\tau}}^{\alpha,(k)}\|} + \|\boldsymbol{p}_{\boldsymbol{\tau}}^{\alpha,(k)} - \gamma_{\boldsymbol{\tau}}\dot{\boldsymbol{u}}_{\boldsymbol{\tau}}^{\alpha,(k)}\|\boldsymbol{I}_2 - \mu p_n^{\alpha,(k)}\boldsymbol{I}_2\Big)(\boldsymbol{p}_{\boldsymbol{\tau}}^{\alpha,(k+1)} - \boldsymbol{p}_{\boldsymbol{\tau}}^{\alpha,(k)}) \\
&= -\|\boldsymbol{p}_{\boldsymbol{\tau}}^{\alpha,(k)} - \gamma_{\boldsymbol{\tau}}\dot{\boldsymbol{u}}_{\boldsymbol{\tau}}^{\alpha,(k)}\|\boldsymbol{p}_{\boldsymbol{\tau}}^{\alpha,(k)} + \mu p_n^{\alpha,(k)}(\boldsymbol{p}_{\boldsymbol{\tau}}^{\alpha,(k)} - \gamma_{\boldsymbol{\tau}}\dot{\boldsymbol{u}}_{\boldsymbol{\tau}}^{\alpha,(k)}).
\end{aligned} \tag{3.45}$$

For recall,

$$\begin{aligned}
\boldsymbol{F}^{(k)} &= \boldsymbol{p}_{\boldsymbol{\tau}}^{\alpha,(k)} \frac{(\boldsymbol{p}_{\boldsymbol{\tau}}^{\alpha,(k)} - \gamma_{\boldsymbol{\tau}}\dot{\boldsymbol{u}}_{\boldsymbol{\tau}}^{\alpha,(k)})^T}{\|\boldsymbol{p}_{\boldsymbol{\tau}}^{\alpha,(k)} - \gamma_{\boldsymbol{\tau}}\dot{\boldsymbol{u}}_{\boldsymbol{\tau}}^{\alpha,(k)}\|}, \\
E^{(k)} &= \frac{1}{\|\boldsymbol{p}_{\boldsymbol{\tau}}^{\alpha,(k)} - \gamma_{\boldsymbol{\tau}}\dot{\boldsymbol{u}}_{\boldsymbol{\tau}}^{\alpha,(k)}\|}.
\end{aligned}$$

Therefore, after an elementary computation

$$\begin{aligned}
&- \gamma_{\boldsymbol{\tau}} E^{(k)}\Big(\boldsymbol{F}^{(k)} - \mu p_n^{\alpha,(k)}\boldsymbol{I}_2\Big)(\dot{\boldsymbol{u}}_{\boldsymbol{\tau}}^{\alpha,(k+1)} - \dot{\boldsymbol{u}}_{\boldsymbol{\tau}}^{\alpha,(k)}) - \mu E^{(k)}(\boldsymbol{p}_{\boldsymbol{\tau}}^{\alpha,(k)} - \gamma_{\boldsymbol{\tau}}\dot{\boldsymbol{u}}_{\boldsymbol{\tau}}^{\alpha,(k)})p_n^{\alpha,(k+1)} \\
&+ \Big(E^{(k)}(\boldsymbol{F}^{(k)} - \mu p_n^{\alpha,(k)}\boldsymbol{I}_2) + \boldsymbol{I}_2\Big)\boldsymbol{p}_{\boldsymbol{\tau}}^{\alpha,(k+1)} - E^{(k)}\Big(\boldsymbol{F}^{(k)} - \mu p_n^{\alpha,(k)}\boldsymbol{I}_2\Big)\boldsymbol{p}_{\boldsymbol{\tau}}^{\alpha,(k)} = 0.
\end{aligned}$$

Now, let

$$\begin{aligned}
\boldsymbol{M}_{\alpha}^{*(k)} &= E^{(k)}(\boldsymbol{F}^{(k)} - \mu p_n^{\alpha,(k)}\boldsymbol{I}_2), \\
\boldsymbol{h}_{\alpha}^{(k)} &= E^{(k)}\boldsymbol{F}^{(k)}\Big(\boldsymbol{p}_{\boldsymbol{\tau}}^{\alpha,(k)} - \gamma_{\boldsymbol{\tau}}\dot{\boldsymbol{u}}_{\boldsymbol{\tau}}^{\alpha,(k)}\Big).
\end{aligned}$$

Then

$$\begin{aligned}
&- \gamma_{\boldsymbol{\tau}}\boldsymbol{M}_{\alpha}^{*(k)}\dot{\boldsymbol{u}}_{\boldsymbol{\tau}}^{\alpha,(k+1)} - \mu E^{(k)}(\boldsymbol{p}_{\boldsymbol{\tau}}^{\alpha,(k)} - \gamma_{\boldsymbol{\tau}}\dot{\boldsymbol{u}}_{\boldsymbol{\tau}}^{\alpha,(k)})p_n^{\alpha,(k+1)} + \Big(\boldsymbol{I}_2 + \boldsymbol{M}_{\alpha}^{*(k)}\Big)\boldsymbol{p}_{\boldsymbol{\tau}}^{\alpha,(k+1)} \\
&= \boldsymbol{h}_{\alpha}^{(k)} - \mu E^{(k)}(\boldsymbol{p}_{\boldsymbol{\tau}}^{\alpha,(k)} - \gamma_{\boldsymbol{\tau}}\dot{\boldsymbol{u}}_{\boldsymbol{\tau}}^{\alpha,(k)})p_n^{\alpha,(k)}.
\end{aligned}$$

In order to simplify even further the notations, we introduce the following operators:

$$\begin{aligned}
\boldsymbol{L}_{\alpha}^{*(k)} &= -\gamma_{\boldsymbol{\tau}}(\boldsymbol{I}_2 + \boldsymbol{M}_{\alpha}^{*(k)})^{-1}\boldsymbol{M}_{\alpha}^{*(k)}, \\
\boldsymbol{r}_{\alpha}^{*(k)} &= (\boldsymbol{I}_2 + \boldsymbol{M}_{\alpha}^{*(k)})^{-1}\boldsymbol{h}_{\alpha}^{(k)}, \\
\boldsymbol{v}_{\alpha}^{(k)} &= \mu(\boldsymbol{I}_2 + \boldsymbol{M}_{\alpha}^{*(k)})^{-1}E^{(k)}(\boldsymbol{p}_{\boldsymbol{\tau}}^{\alpha,(k)} - \gamma_{\boldsymbol{\tau}}\dot{\boldsymbol{u}}_{\boldsymbol{\tau}}^{\alpha,(k)}).
\end{aligned}$$

And, at last

$$\boldsymbol{L}_\alpha^{*(k)}\dot{\boldsymbol{u}}_{\boldsymbol{\tau}}^{\alpha,(k+1)} - \boldsymbol{v}_\alpha^{(k)} p_n^{\alpha,(k+1)} + \boldsymbol{p}_{\boldsymbol{\tau}}^{\alpha,(k+1)} = \boldsymbol{r}_\alpha^{*(k)} - \boldsymbol{v}_\alpha^{(k)} p_n^{\alpha,(k)}.$$

In this specific problem, and for a two dimensional case, one can obtain a simplified equivalent version of the algorithm. Let $\mathcal{D}_{\mathcal{C}_{\boldsymbol{\tau}}^{\boldsymbol{p}}}^{slip}$ be the generalized derivative of $\mathcal{C}_{\boldsymbol{\tau}}^{\boldsymbol{p}}$ in the slip case

$$\begin{aligned}\mathcal{D}_{\mathcal{C}_{\boldsymbol{\tau}}^{\boldsymbol{p}}}^{slip}(\dot{\boldsymbol{u}}_{\boldsymbol{\tau}}^{\alpha}, \boldsymbol{p}_{\boldsymbol{\tau}}^{\alpha})(\delta\dot{\boldsymbol{u}}_{\boldsymbol{\tau}}^{\alpha}, \delta\boldsymbol{p}_{\boldsymbol{\tau}}^{\alpha}) &= \boldsymbol{p}_{\boldsymbol{\tau}}^{\alpha}\frac{(\boldsymbol{p}_{\boldsymbol{\tau}}^{\alpha} - \gamma_{\boldsymbol{\tau}}\dot{\boldsymbol{u}}_{\boldsymbol{\tau}}^{\alpha})^T}{\|\boldsymbol{p}_{\boldsymbol{\tau}}^{\alpha} - \gamma_{\boldsymbol{\tau}}\dot{\boldsymbol{u}}_{\boldsymbol{\tau}}^{\alpha}\|}(\delta\boldsymbol{p}_{\boldsymbol{\tau}}^{\alpha} - \delta\dot{\boldsymbol{u}}_{\boldsymbol{\tau}}^{\alpha}) \\ &- \mu p_n^{\alpha}(\delta\boldsymbol{p}_{\boldsymbol{\tau}}^{\alpha} - \gamma_{\boldsymbol{\tau}}\dot{\boldsymbol{u}}_{\boldsymbol{\tau}}^{\alpha}) + \|\boldsymbol{p}_{\boldsymbol{\tau}}^{\alpha} - \gamma_{\boldsymbol{\tau}}\dot{\boldsymbol{u}}_{\boldsymbol{\tau}}^{\alpha}\|\delta\boldsymbol{p}_{\boldsymbol{\tau}}^{\alpha}.\end{aligned} \tag{3.46}$$

Denoting by $\boldsymbol{\tau}$, the unit slip vector, we have

$$\boldsymbol{p}_{\boldsymbol{\tau}}^{\alpha} = \mu p_n^{\alpha}\boldsymbol{\tau}, \tag{3.47}$$

$$\frac{(\boldsymbol{p}_{\boldsymbol{\tau}}^{\alpha} - \gamma_{\boldsymbol{\tau}}\dot{\boldsymbol{u}}_{\boldsymbol{\tau}}^{\alpha})}{\|\boldsymbol{p}_{\boldsymbol{\tau}}^{\alpha} - \gamma_{\boldsymbol{\tau}}\dot{\boldsymbol{u}}_{\boldsymbol{\tau}}^{\alpha}\|} = \boldsymbol{\tau}, \tag{3.48}$$

$$\delta\boldsymbol{p}_{\boldsymbol{\tau}}^{\alpha} - \gamma_{\boldsymbol{\tau}}\dot{\boldsymbol{u}}_{\boldsymbol{\tau}}^{\alpha} = \eta\boldsymbol{\tau}. \tag{3.49}$$

Combining (3.46)–(3.49), we get

$$\mathcal{D}_{\mathcal{C}_{\boldsymbol{\tau}}^{\boldsymbol{p}}}^{slip}(\dot{\boldsymbol{u}}_{\boldsymbol{\tau}}^{\alpha}, \boldsymbol{p}_{\boldsymbol{\tau}}^{\alpha})(\delta\dot{\boldsymbol{u}}_{\boldsymbol{\tau}}^{\alpha}, \delta\boldsymbol{p}_{\boldsymbol{\tau}}^{\alpha}) = \mu p_n^{\alpha}\eta(\boldsymbol{\tau}\boldsymbol{\tau}^T - \boldsymbol{I}_2)\boldsymbol{\tau} + \|\boldsymbol{p}_{\boldsymbol{\tau}}^{\alpha} - \gamma_{\boldsymbol{\tau}}\dot{\boldsymbol{u}}_{\boldsymbol{\tau}}^{\alpha}\|\delta\boldsymbol{p}_{\boldsymbol{\tau}}^{\alpha}. \tag{3.50}$$

Since $\boldsymbol{\tau}\boldsymbol{\tau}^T + \mathbf{n}\mathbf{n}^{\mathbf{T}} = \boldsymbol{I_2}$ in the 2D case, we have $(\boldsymbol{\tau}\boldsymbol{\tau}^T - \boldsymbol{I}_2)\boldsymbol{\tau} = \mathbf{n}\mathbf{n}^{\mathbf{T}}\boldsymbol{\tau} = \mathbf{0}$. Using (3.26), we obtain

$$\begin{aligned}&\|\boldsymbol{p}_{\boldsymbol{\tau}}^{\alpha,(k)} - \gamma_{\boldsymbol{\tau}}\dot{\boldsymbol{u}}_{\boldsymbol{\tau}}^{\alpha,(k)}\|(\boldsymbol{p}_{\boldsymbol{\tau}}^{\alpha,(k+1)} - \boldsymbol{p}_{\boldsymbol{\tau}}^{\alpha,(k)}) \\ &= -\|\boldsymbol{p}_{\boldsymbol{\tau}}^{\alpha,(k)} - \gamma_{\boldsymbol{\tau}}\dot{\boldsymbol{u}}_{\boldsymbol{\tau}}^{\alpha,(k)}\|\boldsymbol{p}_{\boldsymbol{\tau}}^{\alpha,(k)} + \mu p_n^{\alpha,(k)}(\boldsymbol{p}_{\boldsymbol{\tau}}^{\alpha,(k)} - \gamma_{\boldsymbol{\tau}}\dot{\boldsymbol{u}}_{\boldsymbol{\tau}}^{\alpha,(k)}),\end{aligned} \tag{3.51}$$

Therefore, (3.51) becomes

$$\boldsymbol{p}_{\boldsymbol{\tau}}^{\alpha,(k+1)} = \mu p_n^{\alpha,(k)}\frac{(\boldsymbol{p}_{\boldsymbol{\tau}}^{\alpha,(k)} - \gamma_{\boldsymbol{\tau}}\dot{\boldsymbol{u}}_{\boldsymbol{\tau}}^{\alpha,(k)})}{\|\boldsymbol{p}_{\boldsymbol{\tau}}^{\alpha,(k)} - \gamma_{\boldsymbol{\tau}}\dot{\boldsymbol{u}}_{\boldsymbol{\tau}}^{\alpha,(k)}\|}. \tag{3.52}$$

Finally, the slip 2D conditions of the semi-smooth Newton formalism are as follows

$$\dot{u}_n^{\alpha,(k+1)} = 0, \tag{3.53}$$

$$\boldsymbol{p}_{\boldsymbol{\tau}}^{\alpha,(k+1)} = \mu p_n^{\alpha,(k)}\frac{(\boldsymbol{p}_{\boldsymbol{\tau}}^{\alpha,(k)} - \gamma_{\boldsymbol{\tau}}\dot{\boldsymbol{u}}_{\boldsymbol{\tau}}^{\alpha,(k)})}{\|\boldsymbol{p}_{\boldsymbol{\tau}}^{\alpha,(k)} - \gamma_{\boldsymbol{\tau}}\dot{\boldsymbol{u}}_{\boldsymbol{\tau}}^{\alpha,(k)}\|}. \tag{3.54}$$

4. Non Smooth Contact Dynamics (NSCD)

As seen previously, the unilateral contact between rigid bodies involves a non-smoothness in law between the impulse force and the local relative velocity due to the shock because of friction, and a temporal non-smoothness because of the velocity jumps before and after shock. The Non-Smooth Contact Dynamics (NSCD) approach, based on two main computational level tasks, enables to solve the full problem. Indeed, the global level is devoted to solve the equations of motion, whereas the local level treats the contacts separately. Therefore, it is possible to solve, over a time step, many simultaneous contacts. The main purpose of this section, after presenting the equations of motion, is to come up with a general algorithm for NSCD for which the unilateral contact conditions with dry friction seen in (2.2)–(2.6) are treated numerically by several numerical methods.

4.1. Equations of motion

To describe the motion of a multi-contact system between rigid bodies, we use the following writing conventions. Assuming that a particle P among N_p particles is described by the position of its center of gravity, we will denote by $\boldsymbol{q}$ the generalized coordinate describing its position in space, ($q \in \mathbb{R}^{\bar{d}\times N_p}$, where $\bar{d} = 6$ for a 3D problem and $\bar{d} = 3$ for a 2D problem). As a consequence of the possible shocks between particles, we introduce the generalized velocity denoted by $\dot{\boldsymbol{q}}$ as a function of bounded variations, and its associated differential $d\dot{\boldsymbol{q}}$. According to the fundamental principle of dynamics, the equations of motion formulated in terms of differential measures can be written as follows:

$$\mathbb{M}d\dot{\boldsymbol{q}} + \boldsymbol{F}^{int}(t, \boldsymbol{q}, \dot{\boldsymbol{q}})dt = \boldsymbol{F}^{ext}(t, \boldsymbol{q}, \dot{\boldsymbol{q}})dt + d\boldsymbol{R} \tag{4.1}$$

where

- $\mathbb{M}$ represents the genralized mass matrix;
- $\boldsymbol{F}^{int}$ et $\boldsymbol{F}^{ext}$ represent the internal and external forces respectively;
- $d\boldsymbol{R}$ is a non-negative real measure, representing the reaction forces and impulses between particles in contact.

For the sake of simplicity and without lost of generality, only the external forces are considered in the following.

Considering that the time interval of interest is $[0, T]$, we discretize for numerical purposes the previous equation (4.1). For that, we introduce uniform time instants t_k defined by $t_{k+1} = t_k + \Delta t \; pour \; k = 0, ..., N_T - 1$, where

- $\Delta t = T/N_T$ is the time step;
- N_T is the number of time steps.

The equation (4.1) is then integrated on each time interval $[t_k, t_{k+1}]$ and approximated using a θ-scheme, with $\theta \in [\frac{1}{2}, 1]$ for stability reasons (see [8], [10]). Therefore, the classical approximation of equation (4.1) yields

$$\begin{cases} \mathbb{M}(\dot{\boldsymbol{q}}_{k+1} - \dot{\boldsymbol{q}}_k) = \Delta t(\theta \boldsymbol{F}_{k+1} + (1-\theta)\boldsymbol{F}_k) + \boldsymbol{P}_{k+1}, \\ \boldsymbol{q}_{k+1} = \boldsymbol{q}_k + \Delta t\theta \dot{\boldsymbol{q}}_{k+1} + \Delta t(1-\theta)\dot{\boldsymbol{q}}_k. \end{cases} \tag{4.2}$$

where

- $\boldsymbol{P}_{k+1}$ represents the value of the total impulsion over the time step;
- $\boldsymbol{F}_k$ (resp. $\boldsymbol{F}_{k+1}$) is the external force computed at time t_k (resp. t_{k+1}).

Denoting by $\dot{\boldsymbol{q}}_k^{free} = \dot{\boldsymbol{q}}_k + \mathbb{M}^{-1}\Delta t(\theta \boldsymbol{F}_{k+1} + (1-\theta)\boldsymbol{F}_k)$, the velocity when the contact impulses vanish, the first equation of (4.2) becomes

$$\dot{\boldsymbol{q}}_{k+1} = \dot{\boldsymbol{q}}_k^{free} + \mathbb{M}^{-1}\boldsymbol{P}_{k+1} \tag{4.3}$$

4.2. Local-global mapping

In Non-Smooth Contacts Dynamics NSCD, the contact impulses are not explicit functions which define the state of equilibrium of the studied system. Therefore, contact impulses and velocities must be determined at the same time. As the contact law is expressed using the contact variables, we have to express the equations of motion using these same variables. Thus, a local-global mapping

is defined from the global frame to the local one for each contact node $\alpha \in [1, N_\alpha]$ (where N_α is the total number of potential contacts between two rigid particles) to write the local contact law related. Local relative velocities u_n^α and $u_{\boldsymbol{\tau}}^\alpha$ between the two rigid bodies involved in the contact α can be grouped in a column vector $u \in \mathbb{R}^{d \times N_c}$ (where $d = 3$ for a 3D problem and $d = 2$ for a 2D problem). Likewise, the local contact impulses $\boldsymbol{p^\alpha}$ are represented by a vector $\boldsymbol{p} \in \mathbb{R}^{d \times N_c}$. We recall that $\boldsymbol{p^\alpha}$ can be decomposed into the sum of a normal component p_n^α and a tangential component $\boldsymbol{p_\tau^\alpha}$ as follows: $\boldsymbol{p^\alpha} = p_n^\alpha \boldsymbol{n} + \boldsymbol{p_\tau^\alpha}$. From there, the idea would be to transform the equations of motion seen in (4.2) from $\boldsymbol{P}$ and $\dot{\boldsymbol{q}}$ to $\boldsymbol{p}$ and $\dot{\boldsymbol{u}}$.

For the sake of simplicity and to lighten the notations, the equations of motion (4.2) are converted into a single matrix equation whose expression is as follows:

$$\mathbb{M}(\dot{\boldsymbol{q}}^+ - \dot{\boldsymbol{q}}^-) = \Delta t(\boldsymbol{F} + \boldsymbol{F}_{ext}) \tag{4.4}$$

The contact and particles velocities ($\dot{\boldsymbol{u}}$ and $\dot{\boldsymbol{q}}$) being linearly related, the local-global mapping to compute $\dot{\boldsymbol{u}}$ to $\dot{\boldsymbol{q}}$ at a contact node α is:

$$\dot{\boldsymbol{u}}^\alpha = H^*(\boldsymbol{q}, \alpha)\dot{\boldsymbol{q}} \tag{4.5}$$

where $H^*(\boldsymbol{q}, \alpha)$ local-global mapping matrix $dN_c \times \bar{d}N_p$ carrying the information on the geometry of the contact network. Identically, we have

$$\boldsymbol{P} = H(\boldsymbol{q}, \alpha)\boldsymbol{p}^\alpha \tag{4.6}$$

where $H(\boldsymbol{q}, \alpha)$ is the transpose of matrix $H^*(\boldsymbol{q}, \alpha)$. Since the local-global mapping is computed for each contact node α, the total local-global mapping $\mathbb{H}(\boldsymbol{q}, \alpha)$ allows to compute all velocities and contact impulses from the global to the local frame:

$$\begin{cases} \dot{\boldsymbol{u}} = \mathbb{H}^*(\boldsymbol{q})\dot{\boldsymbol{q}}, \\ \boldsymbol{P} = \mathbb{H}(\boldsymbol{q})\boldsymbol{p}. \end{cases} \tag{4.7}$$

By combining (4.2) and (4.7), the discretization of the multi-contact system's motion, with contact between rigid bodies can be written:

$$\begin{cases} \tilde{\dot{\boldsymbol{u}}}_{k+1} = \tilde{\dot{\boldsymbol{u}}}_k^{free} + \mathbb{W}\boldsymbol{p}_{k+1}, \\ contact\_law(\tilde{u}_{n,k+1}^\alpha, p_{n,k+1}^\alpha) = .true. \quad \forall \alpha \in [1, ..., N_\alpha], \\ friction\_law(\tilde{\dot{\boldsymbol{u}}}_{k+1}^\alpha, \boldsymbol{p}_{k+1}^\alpha) = .true. \quad \forall \alpha \in [1, ..., N_\alpha]. \end{cases} \tag{4.8}$$

4.3. General algorithm for NSCD: Non-Linear Gauss Seidel Method (NLGS)

This paragraph is devoted to the detailed description of the algorithm used at the global level to solve the multi-rigid-body dynamic contact problems ([14]). Following the ideas of Jean and Moreau (see for example [7], [45] , [42]), we use the NLGS algorithm which consists in considering successively each contact until the convergence. The time- stepping method combined with the NLGS algorithm takes the following form:

- Loop on the step time k
  - Prediction of a position (for the computation of the local-global mapping):

$$\mathbf{q}_{k+\frac{1}{2}} = \mathbf{q}_k + \frac{\Delta t}{2}\dot{\mathbf{q}}_k; \tag{4.9}$$

  - Initialization of the motion: $\dot{\mathbf{q}}_{k+1}^0 = \dot{\mathbf{q}}_k^{free}$(initialization of the contact impulses with $\mathbf{P} = 0$).

- Loop on $j \geq 0$ (NLGS), until convergence
  - Loop on the contacts α:
    - Computation of the local-global mapping

$$\dot{\mathbf{u}}^{-} = H^{*}(\mathbf{q}_{k+\frac{1}{2}}, \alpha)\dot{\mathbf{q}}_{k} \; ; \tag{4.10}$$

$$\dot{\mathbf{u}}^{\alpha,j^{+}} = H^{*}(\mathbf{q}_{k+\frac{1}{2}}, \alpha)\dot{\mathbf{q}}^{j}_{k+1} \tag{4.11}$$

    - Newton shock law (using formal Moreau velocity)

$$\tilde{\dot{u}}_{n}^{\alpha,j+1} = \frac{\dot{u}_{n}^{\alpha,j^{+}} + e_{n}\dot{u}_{n}^{-}}{1+e_{n}} \; ; \tag{4.12}$$

$$\tilde{\dot{\boldsymbol{u}}}_{\boldsymbol{\tau}}^{\alpha,j+1} = \frac{\dot{\mathbf{u}}_{\boldsymbol{\tau}}^{\alpha,j^{+}} + e_{n}\dot{\mathbf{u}}_{\boldsymbol{\tau}}^{-}}{1+e_{\boldsymbol{\tau}}} \tag{4.13}$$

    - Computation of the frictional contact law:

$$\begin{cases} contact\_law(\tilde{\dot{u}}_{n}^{\alpha,j+1}, p_{n}^{\alpha,j+1}) = .true. \\ friction\_law(\tilde{\dot{\boldsymbol{u}}}^{\alpha,j+1}, \boldsymbol{p}^{\alpha,j+1}) = .true. \end{cases} \tag{4.14}$$

    - Actualization of the generalized displacement:

$$\dot{\mathbf{q}}^{j+1}_{k+1} = \dot{\mathbf{q}}^{j}_{k+1} + \mathbb{M}^{-1}P(\mathbf{q}_{k+\frac{1}{2}}, \alpha)\boldsymbol{p}^{\alpha,j+1}.$$

  - End of the loop on contacts α.

- End of the loop on j of NLGS. When the convergence is reached, actualization of the velocity: $\dot{\mathbf{q}}_{k+1} = \dot{\mathbf{q}}^{j+1}_{k+1}$
- Actualization of the generalized displacements: $\mathbf{q}_{k+1} = \mathbf{q}_{k+\frac{1}{2}} + \frac{\Delta t}{2}\dot{\mathbf{q}}_{k+1}$

- End of the loop on the step time k.

Remark 1. *The numerical solutions of both "Exact" and "Iterative" methods end the NLGS loop at each time step when convergence is reached. In other words, when the contact impulses are computed on each contact node at the current time step, a stopping criterion is used to exit the non-linear loop. This criterion can be stated as follows:*

$$\max_{\alpha}|p_{n}^{\alpha,j+1}| + \max_{\alpha}|\boldsymbol{p}_{\boldsymbol{\tau}}{}^{\alpha,j+1}| < \epsilon_{NLGS} \tag{4.15}$$

where:

- $p_{n}^{\alpha,j+1}$ *is the normal component of the contact impulse computed at the end of the NLGS loop,*
- $\boldsymbol{p}_{\boldsymbol{\tau}}{}^{\alpha,j+1}$ *is the tangential component of the contact impulse computed at the end of the NLGS loop.*

5. A Primal-Dual Active Set method for NSCD

This section is devoted to the numerical treatment of the contact conditions using a Primal-Dual Active Set method within the framework of multi-rigid-body dynamic contact problems. After defining the active and inactive subsets of all nodes that are currently in contact, we compute the contact conditions on each subset only in terms of contact impulses, using the local general equations of motion (4.8) in the form of (3.1) and (3.2).

5.1. "Exact" Primal-Dual Active Set method (EPDAS)

Let us denote by $\mathcal{S}$ the set of potential contact between particles of the granular material and α a potential contact node between two particles belonging to $\mathcal{S}$. The frictional contact condition (2.2)–(2.6) are realized by applying an active set strategy which derives directly from the computation of the fixed point on the non-linear complementary functions $\mathcal{C}_n^{\boldsymbol{p}}$ and $\mathcal{C}_{\boldsymbol{\tau}}^{\boldsymbol{p}}$ based on the Newton semi-smooth scheme derived in part 3. The active and inactive sets are defined as follows

$$\begin{aligned}
\mathcal{A}_n^{j+1} &= \{\alpha \in \mathcal{S} : p_n^{\alpha,j} - \gamma_n \dot{u}_n^{\alpha,j} \geq 0\},\\
\mathcal{I}_n^{j+1} &= \{\alpha \in \mathcal{S} : p_n^{\alpha,j} - \gamma_n \dot{u}_n^{\alpha,j} < 0\},\\
\mathcal{A}_{\boldsymbol{\tau}}^{j+1} &= \{\alpha \in \mathcal{S} : \|\boldsymbol{p}_{\boldsymbol{\tau}}^{\alpha,j} - \gamma_{\boldsymbol{\tau}} \dot{\boldsymbol{u}}_{\boldsymbol{\tau}}^{\alpha,j}\| - \mu p_n^{\alpha,j} \geq 0\},\\
\mathcal{I}_{\boldsymbol{\tau}}^{j+1} &= \{\alpha \in \mathcal{S} : \|\boldsymbol{p}_{\boldsymbol{\tau}}^{\alpha,j} - \gamma_{\boldsymbol{\tau}} \dot{\boldsymbol{u}}_{\boldsymbol{\tau}}^{\alpha,j}\| - \mu p_n^{\alpha,j} \leq 0\}.
\end{aligned}$$

The status of a given potential α at the non-linear iteration j depends on the set it belongs to. According to part 3, it can be either in the non-contact, slip or stick status.

Hereafter, the numerical computation of the local contact step inside the NLGS iteration loop of index j leads to the following Primal-Dual Active Set algorithm.

(i) Choose $(\dot{\boldsymbol{u}}^{(0)}, \boldsymbol{p}^{(0)})$, $\gamma_n > 0$, $\gamma_{\boldsymbol{\tau}} > 0$ and set $j = 0$.

(ii) Set the active and inactive sets:

$$\begin{aligned}
\mathcal{A}_n^{j+1} &= \{\alpha \in \mathcal{S} : p_n^{\alpha,j} - \gamma_n \dot{u}_n^{\alpha,j} \geq 0\},\\
\mathcal{I}_n^{j+1} &= \mathcal{S} \setminus \mathcal{A}_n^{j+1},\\
\mathcal{A}_{\boldsymbol{\tau}}^{j+1} &= \{\alpha \in \mathcal{S} : \|\boldsymbol{p}_{\boldsymbol{\tau}}^{\alpha,j} - \gamma_{\boldsymbol{\tau}} \dot{\boldsymbol{u}}_{\boldsymbol{\tau}}^{\alpha,j}\| - \mu p_n^{\alpha,j} \geq 0\},\\
\mathcal{I}_{\boldsymbol{\tau}}^{j+1} &= \mathcal{S} \setminus \mathcal{A}_{\boldsymbol{\tau}}^{j+1}.
\end{aligned}$$

(iii) Find $(\dot{\boldsymbol{u}}^{(j+1)}, \boldsymbol{p}^{(j+1)})$ such that

$$p_n^{\alpha,j+1} = 0, \quad \boldsymbol{p}_{\boldsymbol{\tau}}^{\alpha,j+1} = \boldsymbol{0} \qquad \text{for all} \qquad \alpha \in \mathcal{I}_n^{j+1}, \tag{5.1}$$

$$\dot{u}_n^{\alpha,j+1} = 0 \qquad \text{for all} \qquad \alpha \in \mathcal{A}_n^{j+1}, \tag{5.2}$$

$$\boldsymbol{p}_{\boldsymbol{\tau}}^{\alpha,j+1} = \mu p_n^{\alpha,j} \frac{(\boldsymbol{p}_{\boldsymbol{\tau}}^{\alpha,j} - \gamma_{\boldsymbol{\tau}} \dot{\boldsymbol{u}}_{\boldsymbol{\tau}}^{\alpha,j})}{\|\boldsymbol{p}_{\boldsymbol{\tau}}^{\alpha,j} - \gamma_{\boldsymbol{\tau}} \dot{\boldsymbol{u}}_{\boldsymbol{\tau}}^{\alpha,j}\|} \qquad \text{for all} \qquad \alpha \in \mathcal{A}_{\boldsymbol{\tau}}^{j+1} \cap \mathcal{A}_n^{j+1}, \tag{5.3}$$

$$\boldsymbol{p}_{\boldsymbol{\tau}}^{\alpha,j+1} + \frac{\frac{p_n^{\alpha,j+1}}{p_n^{\alpha,j}} \dot{\boldsymbol{u}}_{\boldsymbol{\tau}}^{\alpha,j}}{\mathcal{W}_{\boldsymbol{\tau}\boldsymbol{\tau}}} = \boldsymbol{p}_{\boldsymbol{\tau}}^{\alpha,j} \qquad \text{for all} \qquad \alpha \in \mathcal{I}_{\boldsymbol{\tau}}^{j+1} \cap \mathcal{A}_n^{j+1}. \tag{5.4}$$

(iv) If $\|(\dot{\boldsymbol{u}}^{j+1}, \boldsymbol{p}^{j+1}) - (\dot{\boldsymbol{u}}^{j}, \boldsymbol{p}^{j})\| \leq \epsilon$, $\mathcal{A}_n^{j+1} = \mathcal{A}_n^{j}$ and $\mathcal{A}_{\boldsymbol{\tau}}^{j+1} = \mathcal{A}_{\boldsymbol{\tau}}^{j}$ stop, else goto (ii).

5.2. "Iterative" Primal-Dual Active Set method (IPDAS)

Since we have noticed that (5.4) can lead to numerical instabilities when $p_n^{\alpha,j}$ is small, we introduce a variant of the previous method. Then, the condition (5.4) leads to $\boldsymbol{p}_{\boldsymbol{\tau}}^{\alpha,j+1} + \frac{\dot{\boldsymbol{u}}_{\boldsymbol{\tau}}^{\alpha,j}}{\mathbb{W}_{\boldsymbol{\tau}\boldsymbol{\tau}}} = \boldsymbol{p}_{\boldsymbol{\tau}}^{\alpha,j}$.

Hereafter, the numerical computation of the local contact step inside the NLGS iteration loop of index j leads to the following Primal-Dual Active Set algorithm.

(i) Choose $(\dot{\boldsymbol{u}}^{(0)}, \boldsymbol{p}^{(0)})$, $\gamma_n > 0$, $\gamma_{\boldsymbol{\tau}} > 0$ and set $j = 0$.

(ii) Set the active and inactive sets:

$$\begin{aligned}
\mathcal{A}_n^{j+1} &= \{\alpha \in \mathcal{S} : p_n^{\alpha,j} - \gamma_n \dot{u}_n^{\alpha,j} \geq 0\},\\
\mathcal{I}_n^{j+1} &= \mathcal{S} \setminus \mathcal{A}_n^{j+1},\\
\mathcal{A}_{\boldsymbol{\tau}}^{j+1} &= \{\alpha \in \mathcal{S} : \|\boldsymbol{p}_{\boldsymbol{\tau}}^{\alpha,j} - \gamma_{\boldsymbol{\tau}} \dot{\boldsymbol{u}}_{\boldsymbol{\tau}}^{\alpha,j}\| - \mu p_n^{\alpha,j} \geq 0\},\\
\mathcal{I}_{\boldsymbol{\tau}}^{j+1} &= \mathcal{S} \setminus \mathcal{A}_{\boldsymbol{\tau}}^{j+1}.
\end{aligned}$$

(iii) Find $(\dot{\boldsymbol{u}}^{j+1}, \boldsymbol{p}^{j+1})$ such that

$$p_n^{\alpha,j+1} = 0, \quad \boldsymbol{p}_{\boldsymbol{\tau}}^{\alpha,j+1} = \boldsymbol{0} \qquad \text{for all} \qquad \alpha \in \mathcal{I}_n^{j+1}, \tag{5.5}$$

$$\dot{u}_n^{\alpha,j+1} = 0 \qquad \text{for all} \qquad \alpha \in \mathcal{A}_n^{j+1}, \tag{5.6}$$

$$\boldsymbol{p}_{\boldsymbol{\tau}}^{\alpha,j+1} = \mu p_n^{\alpha,j} \frac{(\boldsymbol{p}_{\boldsymbol{\tau}}^{\alpha,j} - \gamma_{\boldsymbol{\tau}} \dot{\boldsymbol{u}}_{\boldsymbol{\tau}}^{\alpha,j})}{\|\boldsymbol{p}_{\boldsymbol{\tau}}^{\alpha,j} - \gamma_{\boldsymbol{\tau}} \dot{\boldsymbol{u}}_{\boldsymbol{\tau}}^{\alpha,j}\|} \qquad \text{for all} \qquad \alpha \in \mathcal{A}_{\boldsymbol{\tau}}^{j+1} \cap \mathcal{A}_n^{j+1}, \tag{5.7}$$

$$\boldsymbol{p}_{\boldsymbol{\tau}}^{\alpha,j+1} + \frac{\dot{\boldsymbol{u}}_{\boldsymbol{\tau}}^{\alpha,j}}{W_{\boldsymbol{\tau}\boldsymbol{\tau}}} = \boldsymbol{p}_{\boldsymbol{\tau}}^{\alpha,j} \qquad \text{for all} \qquad \alpha \in \mathcal{I}_{\boldsymbol{\tau}}^{j+1} \cap \mathcal{A}_n^{j+1}. \tag{5.8}$$

(iv) If $\|(\dot{\boldsymbol{u}}^{j+1}, \boldsymbol{p}^{j+1}) - (\dot{\boldsymbol{u}}^{j}, \boldsymbol{p}^{j})\| \leq \epsilon$, $\mathcal{A}_n^{j+1} = \mathcal{A}_n^j$ and $\mathcal{A}_{\boldsymbol{\tau}}^{j+1} = \mathcal{A}_{\boldsymbol{\tau}}^j$ stop, else goto (ii).

Before concluding this section, we may underline one of the most characteristic feature of the active set type method, which is to enforce directly and exactly the contact conditions that are found.

Remark 2. *In the simulations which follow, we will use two well-known and powerful methods to calculate the local contact impulses in the previous algorithm. These are methods based on the work of Alart and Curnier (Standard Augmented Lagrangian (SAL)), Saxcé and Feng (The Standard Bi-Potential (SBP)) and an improvement of the Bi-Potentiel Method (IBP, see [15]), which will allow us to evaluate and compare with the Active Set method. For more detail about these methods, we refer to [18].*

Remark 3. *It should also be noted that only one iteration of the Active set method is computed for each contact at each global iteration of the NLGS loop, as in the case of the IBP method, and contrary to the other methods.*

6. Numerical experiments

The main purpose of this section is to provide several numerical experiments on academic cases to assess the PDAS methods in solving granular media flows. To do so, we consider for the first two simulations the following reference configurations: a single spherical steel ball sliding and rolling on a conveyor belt and another one inside a fixed drum. These two configurations are addressed to outline the ability of the PDAS in enforcing basic mechanical properties as conservation properties, and, since the analytical solution is available for the first case, to compare it with the numerical one. The second part of this section brings the light on the robustness and accuracy of the PDAS methods, by carrying out more complex simulations like the sedimentation of a collection of balls. The computational performances of such method are illustrated by comparing it with two other methods (SAL, IBP). The final numerical experiment focuses on the granular flow in a 2D rotating drum which allows comparisons with experiments.

6.1. One sliding and rolling steel ball on a conveyor belt

As mentioned before, the aim of this first example is to carry out comparisons between numerical and analytical solutions. A spherical steel ball, with a non-vanishing initial horizontal velocity ($v_0 = 1m.s^{-1}$) is placed on a conveyor belt with a constant velocity ($\boldsymbol{V_1} = v_1\boldsymbol{x}$ with $v_1 = 2m.s^{-1}$) as shown in Figure . We provide below a description of the physical settings

$$\begin{aligned}
&\rho = 8000\ Kg/m^3, \quad r = 2.7\,10^{-3}\ m,\\
&x_0 = 0\ m, \quad y_0 = 2.7\,10^{-3}\ m,\\
&g = -9.80665\ m/s^2
\end{aligned}$$

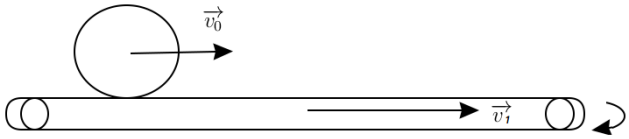

Figure 1: Rolling-Sliding of a steel ball on a plane conveyor belt.

Since there is friction, the steel ball slides until the sliding velocity is zero, then, starts rolling, rolling time $\bar{t}$ being the reference time from which the status of the punctual contact between the ball and the conveyor belt changes. Therefore, we go from sliding to rolling when

$$\bar{t} = \frac{|v_0 - v_1|}{\mu g(1 + \frac{r^2 m}{I})} \tag{6.1}$$

with $I = \frac{2mr^2}{5}$ the moment of inertia of the steel ball. The duration of the simulation is $T = 1s$, and the time step is taken as a sub-multiple of $\bar{t}$. For the numerical experiment, the parameter values are as follows:

$$\begin{aligned}
&T = 1\ s, \quad dt \approx 1.32\,10^{-5}\ s,\\
&e_n = 1.0, \quad e_{\boldsymbol{\tau}} = 1.0, \quad \mu = 0.22,\\
&\gamma_n = 10, \quad \gamma_{\boldsymbol{\tau}} = 10, \quad r_{SAL} = r_{IBP} = \frac{m}{dt}\\
&\text{stopping criterion} : \epsilon_{NLGS} = 10^{-8}
\end{aligned}$$

This simulation is computed with a PDAS method. The numerical solution obtained is then compared to the analytical one in terms of position, angular velocity and rolling velocity.

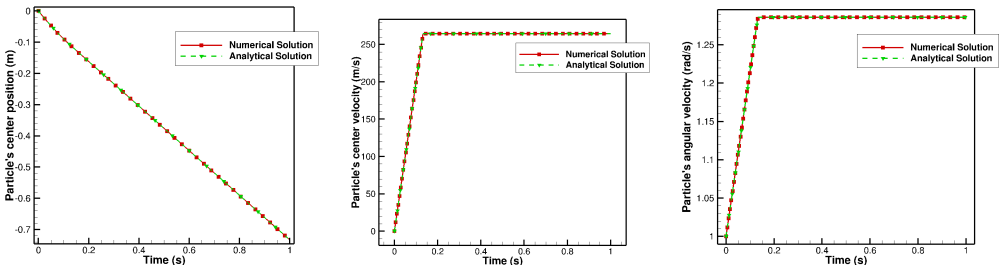

(a) (b) (c)

Figure 2: Comparison between numerical and analytical solution for the sliding-rolling steel ball. (a) Position; (b) Velocity; (c) Angular velocity.

Graphs in Figure 2 clearly show that numerical and analytical curves are the same, both in rolling and sliding steps. Moreover, one can notice (see Table 1) that the absolute error between the numerical and analytical solution for position angular velocity and rolling velocity is is zero, which allows us to validate our model in this case.

Time step	Absolute error on position	Absolute error on angular	Absolute error on velocity
$1.32\,10^{-7}$	$7.83\,10^{-11}$	$1.97\,10^{-8}$	$5.32\,10^{-11}$
$6.62\,10^{-6}$	$2.21\,10^{-11}$	$4.70\,10^{-9}$	$1.27\,10^{-11}$
$1.32\,10^{-6}$	$1.59\,10^{-12}$	$1.44\,10^{-9}$	$3.88\,10^{-12}$
$2.65\,10^{-6}$	$1.73\,10^{-12}$	$1.41\,10^{-9}$	$3.52\,10^{-12}$
$1.32\,10^{-5}$	$5.18\,10^{-13}$	$2.03\,10^{-10}$	$3.83\,10^{-13}$

Table 1: Absolute error between numerical and analytical solution on position, angular velocity and rolling velocity for differents time steps

Concerning the computing time (see Table 2), PDAS, SAL and IBP methods need a similar total CPU time to compute the solution. Moreover, the PDAS methods need only 2 NLGS iterations to converge during the sliding step, 3 for the rolling step, which means that the good status for the contact is directly found. For the SAL method, 20 iterations of NLGS are necessary, and finally, IBP method needs 2 NLGS iterations in both sliding and rolling steps to converge.

Numerical method	NLGS it. (Sliding step)	NLGS it. (Rolling step)	CPU time (s)
$EPDAS$	2	3	0.664
$IPDAS$	2	3	0.692
SAL	20	20	1.584
IBP	2	2	0.744

Table 2: Number of NLGS iterations needed by each method (second column) and total CPU time (third raw) devoted to the computation

6.2. One sliding and rolling steel ball in a fixed drum

Let us consider in this part another representative example, the same steel ball as the previous one, posed inside a fixed drum (see Figure 3), with a non-vanishing initial horizontal velocity ($v_0 = 0.5m.s^{-1}$). We provide below a description of the physical settings:

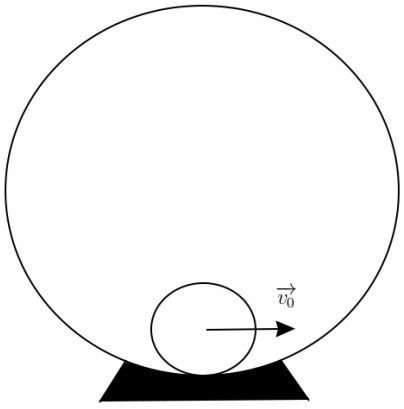

Figure 3: Rolling-Sliding of a steel ball inside a fixed drum.

$$\rho = 8000\ Kg/m^3, \quad r = 2.7\,10^{-3}\ m,$$
$$Fixed\ drum\ radius : 0.05\ m,$$
$$g = -9.80665\ m/s^2$$

The dynamic behavior of the steel ball is similar to a pendulum. Indeed, the steel ball reaches a maximum position, position for which the ball's translational velocity is zero. Moreover, since there is friction, the ball has an angular velocity that varies over time. For the numerical experiment, the parameter values are as follows:

$$T = 5\ s, \quad dt = 2.5\,10^{-5}\ s,$$
$$e_n = 1.0, \quad e_{\boldsymbol{\tau}} = 1.0, \quad \mu = 0.22,$$
$$\gamma_n = 10, \quad \gamma_{\boldsymbol{\tau}} = 10, \quad r_{SAL} = r_{IBP} = \frac{m}{dt}$$
$$\text{stopping criterion} : \epsilon_{NLGS} = 10^{-8}$$

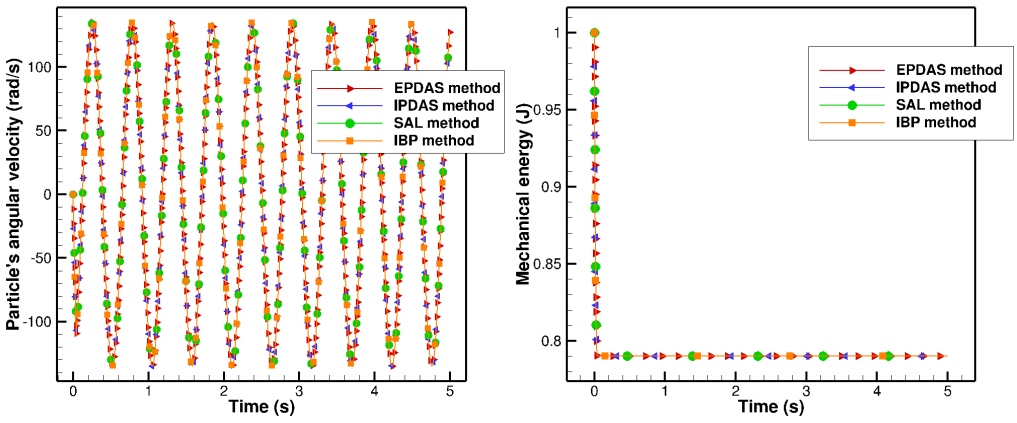

(a) (b)

Figure 4: Evolution of two characteristic variables over time for the sliding-rolling steel ball inside a fixed drum. (a) Particle's angular velocity; (b) Particle's mechanical energy.

Figure 4a describes the evolution of the ball's angular velocity over time during the sliding-rolling process inside the fixed drum. Since there is friction, the steel ball slides until the angular velocity reaches a value of $-110\ rad/s$, then, starts rolling. One can observe that the angular velocity oscillates over time and reaches it's maximum in absolute value. This maximum value does not decrease during the rolling step and reaches the same maximum value, since there is no more friction and the normal restitution coefficient is equal to 1.

Figure 4b shows the evolution of the system's mechanical energy over time during the sliding-rolling process inside the fixed drum. It decreases brutally during the sliding step because of the friction, then it is conserved during the rolling step.

Numerical method	NLGS iterations	CPU time (s)
$EPDAS$	3	1.396
$IPDAS$	3	1.356
SAL	between 30 and 40	5.224
IBP	2	1.844

Table 3: Number of NLGS iterations needed by each method (second column) and total CPU time (third raw) devoted to the computation

On the other hand, it is notable (see Table 3) that all the methods need a similar total CPU time to compute the solution, except from SAL method which is more expensive in terms of computing time. Besides, the PDAS methods need only 3 NLGS iterations to converge, 2 for IBP method, while SAL method need more than 30 NLGS iterations to converge.

6.3. Sedimentation of a collection of balls

We introduce for this third numerical example a representative configuration to show the performances of PDAS methods. The sedimentation of a collection of rigid balls in a box is considered, with particular emphasis on the comparison between the PDAS methods and the standard methods used to compute the local contact impulses. Each rigid ball of the collection has an initial random velocity. Figure 5 illustrates the sedimentation process of 100, 200, 400, 800 and 1600 particles. For each configuration, two different radii are considered for the particles. We provide below the value of the physical settings used for the computation:

$$\begin{aligned}
&\rho = 2600\ Kg/m^3, \quad r = (see\ table\ 4),\\
&Domain\ size : [0, 0.012] \times [0, 0.022]\ m^2,\\
&g = -9.80665\ m/s^2, \quad v_0 = random
\end{aligned}$$

Number of particles	Small radius (m)	Large radius (m)
100	$2.5\,10^{-4}$	$5.0\,10^{-4}$
200	$2.5\,10^{-4}$	$4.5\,10^{-4}$
400	$1.2\,10^{-4}$	$2.6\,10^{-4}$
800	$1.2\,10^{-4}$	$2.3\,10^{-4}$
1600	$6.0\,10^{-5}$	$1.3\,10^{-4}$

Table 4: Radii ranging for each sedimentation's configuration

The simulation is computed over $1s$, the numerical parameters related to this experiment are the following:

$$\begin{aligned}
&T = 1\ s, \quad dt = 10^{-4}\ s,\\
&e_n = 1.0, \quad e_{\boldsymbol{\tau}} = 1.0, \quad \mu = 0.2,\\
&\gamma_n = 10^{-4}, \quad \gamma_{\boldsymbol{\tau}} = 10^{-9}, \quad r_{SAL} = r_{IBP} = \tfrac{m}{dt}\\
&\text{stopping criterion} : \epsilon_{NLGS} = 10^{-6}
\end{aligned}$$

This example is representative of granular flow simulations due to the large number of rigid bodies involved and the large amount of CPU time needed to compute the solution. According to the

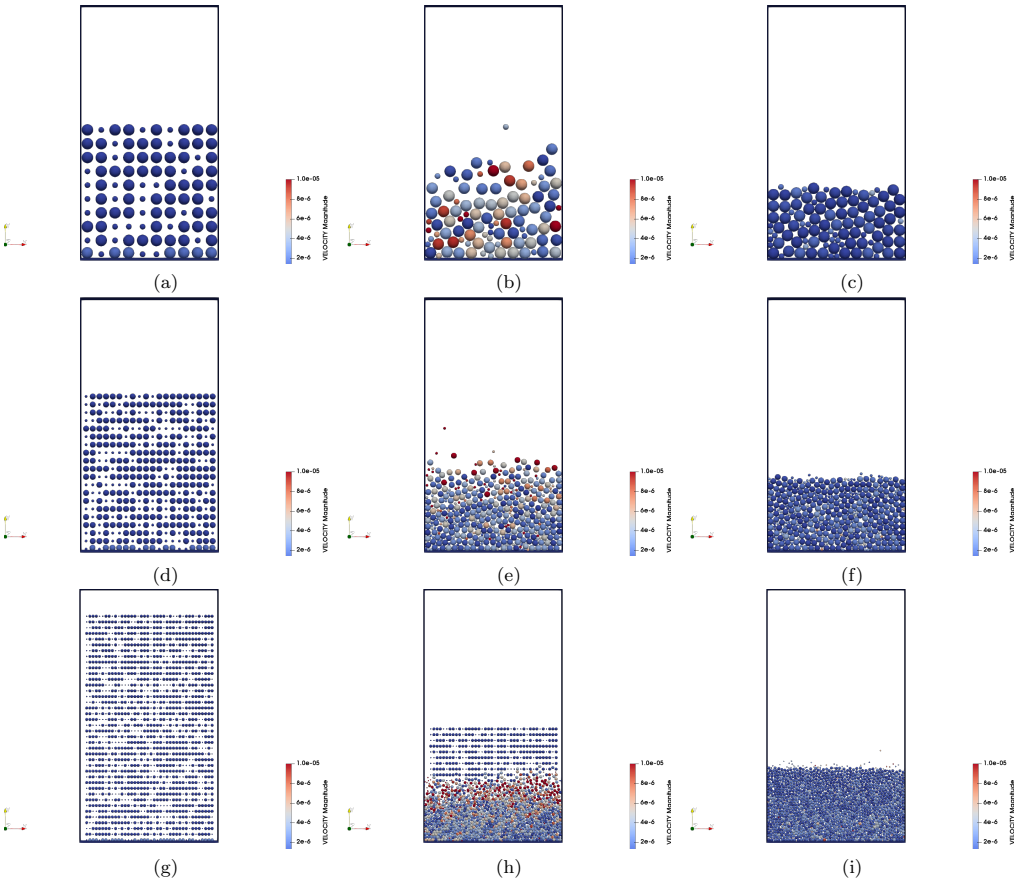

Figure 5: Screenshots of the sedimentation process of a collection of rigid balls in a box over time. [(a), (b), (c)] 100 rigid balls, [(d), (e), (f)] 400 rigid balls, [(g), (h), (i)] 1600 rigid balls.

graphs in Figure 6, one can observe that both EPDAS and IPDAS methods provide the best results in terms of computing time during the whole sedimentation process of 100 and 200 rigid balls in a box. Indeed, the cumulative time required to compute the contact impulses using PDAS method increases slightly over time compared to SAL and IBP methods, which need a larger CPU time to compute the solution. For a large number of particles involved, Table 5 resumes the total CPU time values for each numerical method.

Total CPU time (s)					
Numerical method	100 balls	200 balls	400 balls	800 balls	1600 balls
EPDAS	2.588	8.412	28.347	107.919	12298.419
IPDAS	2.562	8.392	28.347	105.408	11515.381
SAL	22.294	44.214	87.293	$182.144^{(*)}$	$18673.187^{(*)}$
IBP	13.751	33.533	65.856	$186.395^{(*)}$	$16798.548^{(*)}$

Table 5: Total CPU time devoted to the computation of the contact impulses during the sedimentation process for each numerical method and different number of rigid balls.

On the other hand, this numerical experiment assesses not only the performances of PDAS methods, but also the robustness of such methods. Graphs in Figure 7 show the evolution of the cu-

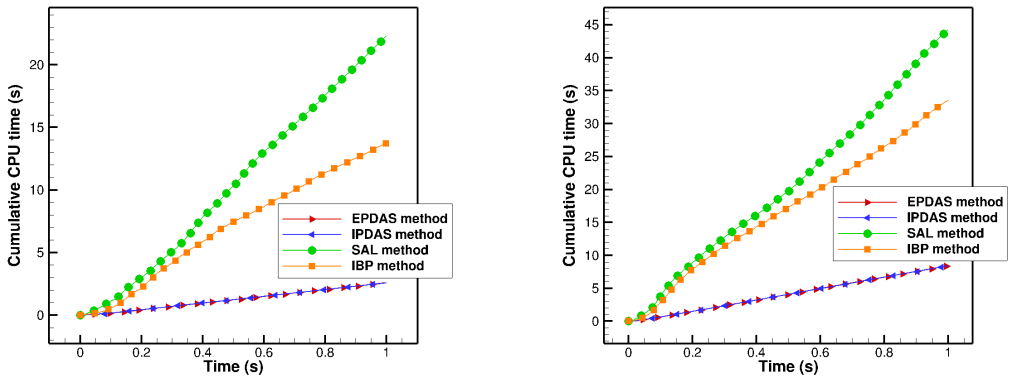

(a) (b)

Figure 6: Evolution of the cumulative CPU time required to compute the contact impulses during the sedimentation process. (a) 100 rigid balls and (b) 200 rigid balls.

mulative NLGS iterations required to the convergence of the contact impulses' computation during the sedimentation process, and it can be noted that both EPDAS and IPDAS curves are quite similar and tend to converge faster than the SAL method, and provide comparable results with IBP method, especially at the end of the sedimentation process. For a large number of particles involved, Table 6 resumes the total NLGS iterations values needed to compute the solution for each numerical method.

Remark 4. *It should be pointed out that results marked with an asterisk in Table 3 correspond to the simulations conducted with SAL and IBP methods where we noticed some large interpenetrations between rigid particles at the end of the sedimentation process.*

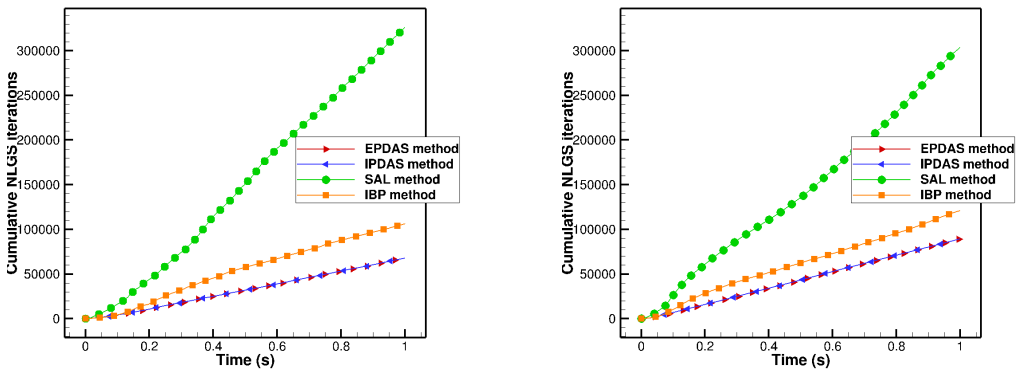

(a) (b)

Figure 7: Evolution of the cumulative NLGS iterations required to the convergence of the contact impulses computation during the sedimentation process. (a) 100 rigid balls and (b) 200 rigid balls.

6.4. Granular materials in a 2D rotating drum

The final numerical example concerns the well-known rotating drum in which we study the behavior of a collection of steel balls in motion. The physical and numerical parameters of the following simulation have been chosen so that it corresponds to the one performed in [46], in order to provide

Total NLGS iterations					
Numerical method	100 balls	200 balls	400 balls	800 balls	1600 balls
EPDAS	67726	89347	95995	147445	25578301
IPDAS	67121	85663	99765	142802	23836195
SAL	326121	363596	442943	$144305^{(*)}$	$2648147^{(*)}$
IBP	106194	120975	138970	$83404^{(*)}$	$1978658^{(*)}$

Table 6: Total NLGS iterations needed to the computation of the contact impulses during the sedimentation process for each numerical method and different number of rigid balls.

a comparison between the experiment achieved and the numerical results. Figure 8 presents screenshots of the experiment produced with 1.5 Kg of steel balls in a rotating drum at 40 rpm and the DEM simulation related. Steel balls tend to organize themselves in layers: one layer in contact with the wall and the rest within the bed. In this study, PDAS methods are performed to evaluate the average rising height and the mean angle of repose during $1s$ of simulation. Beyond the numerical comparison, the interest of this example lies in the fact that such experiment assesses the efficiency and the reliability of PDAS methods.

Several simulations were carried out with PDAS methods in order to measure the corresponding mean angle of repose and the rising height. In that respect, we put 100, 200, 400, 800 and then 1600 steel balls in the rotating drum. First, we provide below a description of the physical settings used for this experiment:

$$
\begin{aligned}
&\textit{Number of particles} : 100 \ / \ 200 \ / \ 400 \ / \ 800 \ / \ 1600,\\
&\textit{Rotational speed} = 40 \ rpm,\\
&\rho = 8000 \ Kg/m^3, \quad r \leq 2.7\,10^{-3} \ m,\\
&\textit{Rotating drum radius} : 0.05 \ m,\\
&g = -9.80665 \ m/s^2,
\end{aligned}
$$

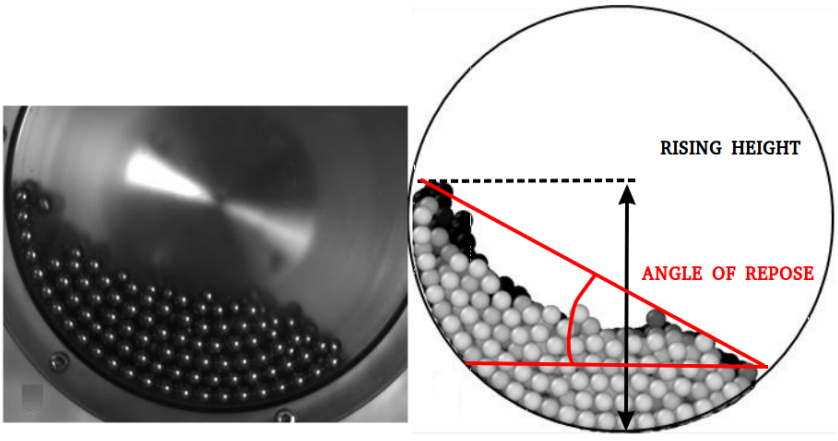

Figure 8: Comparison between the experiment and the DEM simulation performed in [46] with steel balls inside a rotating drum.

The numerical parameters of the rotating drum experiment are as follows:

$$T = 1\ s, \quad dt = 10^{-4}\ s,$$
$$e_n = 0.6, \quad e_{\boldsymbol{\tau}} = 1.0, \quad \mu = 0.22,$$
$$\gamma_n = 10^{-8}, \quad \gamma_{\boldsymbol{\tau}} = 10^{-8}, \quad r_{SAL} = r_{IBP} = \frac{m}{dt}$$
$$\text{stopping criterion} : \epsilon_{NLGS} = 10^{-6}$$

These simulations are also representative of multi-rigid body contact problems due to the large number of rigid balls considered and the large amount of CPU time needed to compute the solution. In Figure 9, one can observe that both of repose angle and rising height achieved by PDAS methods are quite similar to the ones observed in Figure 8, and this regardless of the number of particles involved. According to [46], the resulting angle of repose is equal to 26°.

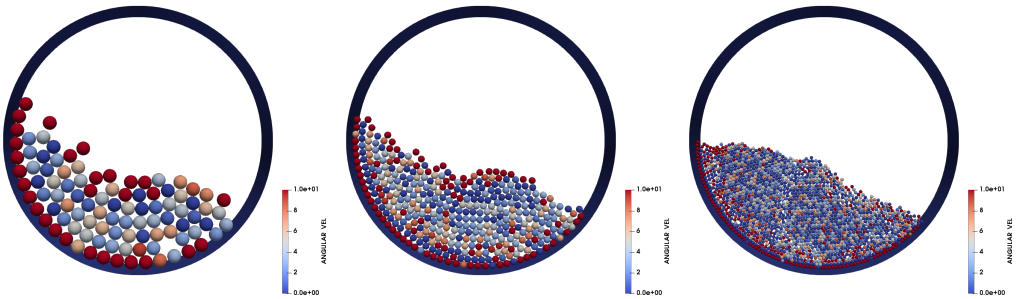

(a) (b) (c)

Figure 9: Perspective views of the rotating drum performed with PDAS methods with (a) 100 steel balls, (b) 400 steel balls, 1600 steel balls

With regard to the convergence of the numerical methods, Graphs in Figure 10 assess once again the efficiency of PDAS methods, that provide very comparable results with IBP method. It is to highlight that both EPDAS and IPDAS curves are quite similar and tend to converge faster than SAL method. For instance, when it comes to deal with 1600 steel balls (see Table 7), the total NLGS iterations needed to compute the whole simulation varies from 8 million to 10 million for PDAS and IBP methods, whereas it takes more than 30 million NLGS iterations to the SAL method to converge.

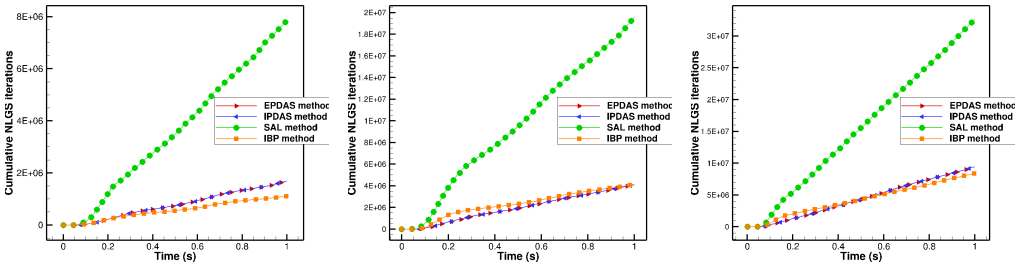

(a) (b) (c)

Figure 10: Evolution of the cumulative time required to compute the contact impulses during the the rotating drum simulation. (a) 100 steel balls, (b) 400 steel balls and (c) 1600 steel balls.

Also, the performances of PDAS methods for such experiments are quite notable comparing to SAL and IBP methods. Below, we provide total CPU times for each simulation and each numerical

Total NLGS iterations					
Numerical method	100 balls	200 balls	400 balls	800 balls	1600 balls
EPDAS	1680882	2020349	4069672	5114280	9422476
IPDAS	1674177	1933869	4036740	5036011	9999666
SAL	7836547	8566285	19607909	15600032	32656132
IBP	1101849	1340917	4121136	3688553	8375264

Table 7: Total NLGS iterations needed to the computation of the rotating drum simulation for each numerical method and different number of steel balls.

method. Regardless of the number of rigid balls involved in the process, PDAS methods remain the least expensive in terms of computing time. Indeed, as we can see from the graphs in Figure 11, the cumulative CPU time required to compute the contact impulses using PDAS methods increases slightly over time compared to SAL and IBP methods. Furthermore, one can notice according to Table 8 that the CPU time strongly depends on the number of rigid balls involved in the simulation. Indeed, the more rigid balls we have in the rotating drum, the more the gap in CPU time widens, making the PDAS methods the most relevant in this example.

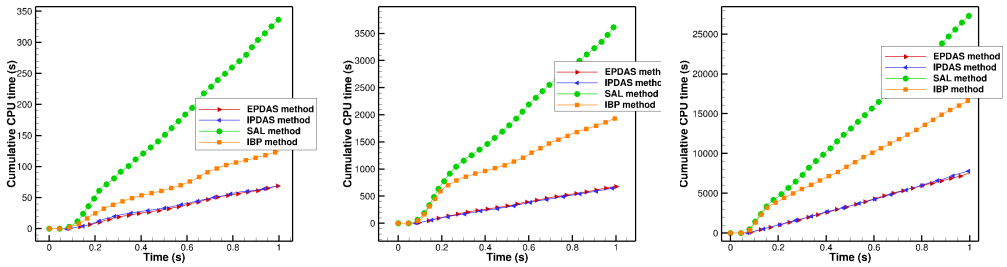

(a) (b) (c)

Figure 11: Evolution of the cumulative CPU time required to compute the contact impulses during the rotating drum simulation. (a) 100 steel balls, (b) 400 steel balls and (c) 1600 steel balls.

Total CPU time (s)					
Numerical method	100 balls	200 balls	400 balls	800 balls	1600 balls
EPDAS	69.482	163.918	677.212	1817.413	7492.300
IPDAS	68.813	153.254	657.011	1804.862	7867.878
SAL	337.16	755.553	3663.254	6055.488	27425.824
IBP	124.918	259.370	1941.158	3232.919	16740.516

Table 8: Total CPU time devoted to the computation of the rotating drum simulation for each method and different number of steel balls.

7. Conclusion

The main contribution of this work consisted of the treatment of frictional contacts within the framework of Active Set method. An adaptation of these methods to solve multi-rigid-body dynamics contact problems has been proposed in the first part of this paper. Indeed, after defining the frictional contact conditions through the NSCD formalism, a general algorithm has been detailed to treat those conditions numerically. A series of academic test cases covering a broad range of granular materials applications has been carried out to assess the relevance of PDAS methods. As a first result, it turns out that their efficiency and speed are better compared to standard and improved methods,

the saving in computing time is considerable. Moreover, the numerical experiments reported above demonstrate that computing times widen and are no longer comparable when the number of rigid bodies involved becomes larger, but still faster for PDAS methods compared to other ones. These promising results push us to extend this work to 3D in order to cover a wide range of industrial applications with complex behaviors. Treating these applications in 3D by means of Active Set type method remains, as far as we know, an open work that will be worth discussing in more details. Furthermore, as the number of rigid bodies will increase considerably, we must give serious thought to parallel computing and show the relevance of PDAS methods in terms of computing time. Continuous effort will be devoted to study the parallelization performances of such methods in future works.

References

[1] P. A. Cundall and O. D. L. Strack. A discrete numerical model for granular assemblies. *Geotechnique*, 29(1):47–65, 1979.

[2] F. Dubois, V. Acary, and M. Jean. The contact dynamics method: A nonsmooth story. *Comptes Rendus Mécanique*, 346(3):247–262, 2018.

[3] F. Radjai and V. Richefeu. Contact dynamics as a nonsmooth discrete element method. *Mechanics of Materials*, 41(6):715–728, 2009.

[4] R. Garg, J. Galvin, T. Li, and S. Pannala. Documentation of open-source mfix–dem software for gas–solids flows. *From URL https://mfix. netl. doe. gov/download/mfix/mfix_current_documentation/dem_doc_2012-1. pdf*, 2012.

[5] JJ. Moreau. Some numerical methods in multibody dynamics: application to granular materials. *European Journal of Mechanics-A/Solids*, 13(4-suppl):93–114, 1994.

[6] M. Jean and JJ. Moreau. Unilaterality and dry friction in the dynamics of rigid body collections. In *1st Contact Mechanics International Symposium*, pages 31–48, 1992.

[7] M. Jean. The non-smooth contact dynamics method. *Computer methods in applied mechanics and engineering*, 177(3-4):235–257, 1999.

[8] JJ. Moreau. Numerical aspects of the sweeping process. *Computer methods in applied mechanics and engineering*, 177(3-4):329–349, 1999.

[9] V. Acary and B. Brogliato. *Numerical methods for nonsmooth dynamical systems: applications in mechanics and electronics*. Springer Science & Business Media, 2008.

[10] M. Renouf and P. Alart. Conjugate gradient type algorithms for frictional multi-contact problems: applications to granular materials. *Computer Methods in Applied Mechanics and Engineering*, 194(18-20):2019–2041, 2005.

[11] M. Renouf, F. Dubois, and P. Alart. A parallel version of the non smooth contact dynamics algorithm applied to the simulation of granular media. *Journal of Computational and Applied Mathematics*, 168(1-2):375–382, 2004.

[12] V. Visseq, P. Alart, and D. Dureisseix. High performance computing of discrete nonsmooth contact dynamics with domain decomposition. *International journal for numerical methods in engineering*, 96(9):584–598, 2013.

[13] G. de Saxcé and Z-Q. Feng. New inequality and functional for contact with friction: the implicit standard material approachâ. *Journal of Structural Mechanics*, 19(3):301–325, 1991.

[14] J. Fortin, O. Millet, and G. de Saxcé. Numerical simulation of granular materials by an improved discrete element method. *International Journal for Numerical Methods in Engineering*, 62(5):639–663, 2005.

[15] Z-Q Feng, P. Joli, J-M Cros, and B. Magnain. The bi-potential method applied to the modeling of dynamic problems with friction. *Computational Mechanics*, 36(5):375–383, 2005.

[16] P. Alart and A. Curnier. A mixed formulation for frictional contact problems prone to newton like solution methods. *Computer methods in applied mechanics and engineering*, 92(3):353–375, 1991.

[17] J. Fortin, M. Hjiaj, and G. de Saxcé. An improved discrete element method based on a variational formulation of the frictional contact law. *Computers and Geotechnics*, 29(8):609–640, 2002.

[18] S. Dumont. On enhanced descent algorithms for solving frictional multicontact problems: application to the discrete element method. *International Journal for Numerical Methods in Engineering*, 93(11):1170–1190, 2013.

[19] P. Joli and Z-Q Feng. Uzawa and newton algorithms to solve frictional contact problems within the bi-potential framework. *International journal for numerical methods in engineering*, 73(3):317–330, 2008.

[20] V. Acary. Projected event-capturing time-stepping schemes for nonsmooth mechanical systems with unilateral contact and coulombâs friction. *Computer Methods in Applied Mechanics and Engineering*, 256:224–250, 2013.

[21] V. Acary. Energy conservation and dissipation properties of time-integration methods for nonsmooth elastodynamics with contact. *ZAMM-Journal of Applied Mathematics and Mechanics/Zeitschrift für Angewandte Mathematik und Mechanik*, 96(5):585–603, 2016.

[22] P. Chabrand, F. Dubois, and M. Raous. Various numerical methods for solving unilateral contact problems with friction. *Mathematical and computer modelling*, 28(4-8):97–108, 1998.

[23] F. Chouly, M. Fabre, P. Hild, R. Mlika, J. Pousin, and Y. Renard. An overview of recent results on Nitsche's method for contact problems. *Geometrically unfitted finite element methods and applications*, pages 93–141, 2017.

[24] H.B Khenous, J. Pommier, and Y. Renard. Hybrid discretization of the signorini problem with Coulomb friction. theoretical aspects and comparison of some numerical solvers. *Applied Numerical Mathematics*, 56(2):163–192, 2006.

[25] F. Lebon. Contact problems with friction: models and simulations. *Simulation Modelling practice and theory*, 11(5-6):449–463, 2003.

[26] T A Laursen. *Computational contact and impact mechanics: fundamentals of modeling interfacial phenomena in nonlinear finite element analysis*. Springer Science & Business Media, 2013.

[27] M. Raous, P. Chabrand, and F. Lebon. Numerical methods for solving unilateral contact problem with friction. *Journal of Theoretical and Applied Mechanics*, 7:111–128, 1988.

[28] M. Sofonea and A. Matei. *Mathematical models in contact mechanics*, volume 398. Cambridge University Press, 2012.

[29] P. Wriggers and G. Zavarise. Computational contact mechanics. *Encyclopedia of computational mechanics*, 2004.

[30] M. Hintermüller, K. Ito, and K. Kunisch. The primal-dual active set strategy as a semismooth Newton method. *SIAM Journal on Optimization*, 13(3):865–888, 2002.

[31] M. Hintermüller, V. A Kovtunenko, and K. Kunisch. *Semismooth Newton methods for a class of unilaterally constrained variational problems*. Universität Graz/Technische Universität Graz. SFB F003-Optimierung und Kontrolle, 2003.

[32] S. Hüeber, G. Stadler, and B. I Wohlmuth. A primal-dual active set algorithm for three-dimensional contact problems with coulomb friction. *SIAM Journal on scientific computing*, 30(2):572–596, 2008.

[33] S. Hüeber and B. I Wohlmuth. A primal–dual active set strategy for non-linear multibody contact problems. *Computer Methods in Applied Mechanics and Engineering*, 194(27-29):3147–3166, 2005.

[34] S. Abide, M. Barboteu, and D. Danan. Analysis of two active set type methods to solve unilateral contact problems. *Applied Mathematics and Computation*, 284:286–307, 2016.

[35] S. Abide, M. Barboteu, S. Cherkaoui, D. Danan, and S. Dumont. Inexact primal–dual active set method for solving elastodynamic frictional contact problems. *Computers & Mathematics with Applications*, 82:36–59, 2021.

[36] F. Chouly. An adaptation of Nitsche's method to the tresca friction problem. *Journal of Mathematical Analysis and Applications*, 411(1):329–339, 2014.

[37] F. Chouly, P. Hild, and Y. Renard. A Nitsche finite element method for dynamic contact: 1. space semi-discretization and time-marching schemes. *ESAIM: Mathematical Modelling and Numerical Analysis*, 49(2):481–502, 2015.

[38] T. Koziara and N. Bićanić. Semismooth Newton method for frictional contact between pseudo-rigid bodies. *Computer Methods in Applied Mechanics and Engineering*, 197(33-40):2763–2777, 2008.

[39] IM. Sharaf. An active set algorithm for a class of linear complementarity problems arising from rigid body dynamics. *Pakistan Journal of Statistics and Operation Research*, pages 339–352, 2016.

[40] M. Barboteu and S. Dumont. A primal-dual active set method for solving multi-rigid-body dynamic contact problems. *Mathematics and Mechanics of Solids*, 23(3):489–503, 2018.

[41] JJ. Moreau. Application of convex analysis to some problems of dry friction. In *Trends in applications of pure mathematics to mechanics*, pages 263–280. Pitman, 1977.

[42] JJ. Moreau. Unilateral contact and dry friction in finite freedom dynamics. In Moreau J.J., Panagiotopoulos P.D. International Centre for Mechanical Sciences (Courses, and Lectures, editors, *Nonsmooth mechanics and Applications*, pages 1–82. Springer, 1988.

[43] A. Signorini. Sopra alcune questioni di elastostatica. *Atti della Societa Italiana per il Progresso delle Scienze*, 27:69, 1933.

[44] Y. Desplanques. Amontons-Coulomb friction laws, a review of the original manuscript. *SAE International Journal of Materials and Manufacturing*, 8(1):98–103, 2015.

[45] F. Jourdan, P. Alart, and M. Jean. A Gauss-Seidel like algorithm to solve frictional contact problems. *Computer methods in applied mechanics and engineering*, 155(1-2):31–47, 1998.

[46] R. Maione, S. Kiesgen De Richter, G. Mauviel, and G. Wild. DEM investigation of granular flow and binary mixture segregation in a rotating tumbler: Influence of particle shape and internal baffles. *Powder Technology*, 286:732–739, 2015.

Funding/Acknowledgements: The project has received funding from the European Commission Horizon 2020 Research and Innovation Programme under the Marie Sklodowska-Curie grant agreement No. 823731 - CONMECH. This work was also realized with the support of HPC@LR, a Center of competence in High-Performance Computing from the Languedoc-Roussillon region.

Declaration of interests

☐ The authors declare that they have no known competing financial interests or personal relationships that could have appeared to influence the work reported in this paper.

☒ The authors declare the following financial interests/personal relationships which may be considered as potential competing interests:

Barboteu reports a relationship with European Commission Horizon 2020 Research and Innovation Programme under the Marie Sklodowska-Curie grant agreement No. 823731 - CONMECH. that includes: funding grants.